Chapter 3

Sintering of the Tricalcium Phosphate-Titania-Magnesium Fluoride Composites

Ibticem Ayadi and Foued Ben Ayed

Additional information is available at the end of the chapter

http://dx.doi.org/10.5772/intechopen.68501

Abstract

Titania (TiO_2) and magnesium fluoride (MgF_2) can be mixed with tricalcium phosphate (β-$Ca_3(PO_4)_2$, β-TCP) to make bioceramic composites, which would combine the biocompatibility of the β-TCP and the high tribological properties of TiO_2 and MgF_2 for biomedical applications. The samples were characterized by different characterization techniques such as physicochemical and mechanical. The sintering of the TCP at various temperatures (1000, 1100, 1200 and 1300°C) with different percentages of titania (2.5, 5, 7.5, 10, 20, 30, 40 and 50 wt%) was studied. The performances of the TCP-TiO_2 composites increase with both the sintering temperature and the amount of titania. The highest values of the composites' (H = 270 Hv; E = 33.1 GPa and G = 15.7 GPa) were obtained with 40 wt% titania at 1200°C. Moreover, the addition of 4 wt% MgF_2 to the TCP-40 wt% TiO_2 composites leads to better mechanical properties (σ_r = 27 MPa; H = 360 Hv; E = 51 GPa and G = 20 GPa) at 1200°C for 1 h. The amelioration of these properties is due to the formation of a new compound and the liquid phase which helps to fill the pores in the microstructure. The obtained performances of the TCP-TiO_2-MgF_2 composites are similar to those of bone tissue and especially as enamel.

Keywords: sintering, biomaterial, composites, mechanical properties, tricalcium phosphate

1. Introduction

Tricalcium phosphate (β-$Ca_3(PO_4)_2$, β-TCP) based on biomaterial has attracted considerable interest for orthopedic and dental applications [1–13]. The tricalcium phosphate has been used clinically to repair bone defects for many years [6–10]. However, the major limitation of the β-TCP uses as load bearing biomaterial is their poor fatigue resistance [6, 9]. Moreover, the mechanical properties of tricalcium phosphate are generally inadequate for many load-carrying

applications [3, 6, 9]. Hence, inert oxides such as alumina (Al_2O_3) or zirconia (ZrO_2) have been widely studied due to their bio-inertness, excellent tribological properties, fracture toughness and strength [6, 9, 11–15]. Thus, the study conducted by Sakka et al. has recently concerned with the tricalcium phosphate/alumina system [11]. The researchers were interested in producing the Al_2O_3-TCP composites with different percentages of β-TCP (10, 20, 40 and 50 wt%). In fact, the best mechanical properties of this study reached 13.5 MPa with a composition of the alumina-10 wt% tricalcium phosphate composite after the sintering at 1600°C [11]. Thereby, the next study directed by Sakka et al. proved that the incorporation of 5 wt% TiO_2 to the alumina-10 wt% tricalcium phosphate composite matrix leads to the highest mechanical performances (74 MPa) at 1600°C [12]. However, the very low content of tricalcium phosphate (10 wt%) in the composites based on alumina, titania and tricalcium phosphate limits its use in the biomedical applications. Furthermore, the presence of the sizeable grains hinders the performances of these composites caused by the high temperature sintering [12]. Also, the study made by Sallemi et al. was interested to elaborate and to characterize the tricalcium phosphate-zirconia composites with different percentages of zirconia (25, 50 and 75 wt%) [14]. Thus, the ultimate values of the performances of the tricalcium phosphate were obtained with 50 wt% zirconia [14]. But, the experimental results in this study indicate the appearance of low mechanical properties of the tricalcium phosphate-zirconia composites [13, 14]. Based on the results, the inverse allotropic transformation of zirconia is sufficient to cause the degradation of mechanical properties of these composites [13, 14]. Thus, the expansion in volume of the zirconia samples is responsible for the fragility of the tricalcium phosphate-zirconia composites [13, 14]. In conclusion, the addition of alumina or zirconia to the TCP matrix did not enhance the mechanical properties [11–14]. For this reason, we tested another inert oxide like titania (TiO_2). Besides, titania has attracted much attention due to its excellent ability to chemically bond with living hard tissue [16, 17]. This happens through the formation of a bone mineral, such as tricalcium phosphate phase on the material surface that ultimately induces direct bonding with native bone tissue [18–20]. Thus, titania has been attracting attention as an implantable material because it is harmless to a living body, and with good mechanical properties. Moreover, titania is an attractive material, applicable to various fields, such as biomedical applications [16–20]. Furthermore, the titania is considered as having excellent biocompatibility, manifested in various biomedical applications [16–20]. So, the choice of the titania added to the tricalcium phosphate matrix was based on those considerations. Thereby, we would combine the biocompatibility of the TCP with the high mechanical and tribological properties of titania in order to elaborate a bioceramic composite. This combination of calcium phosphate/inert oxide system could give rise to more biomaterials in the physiological environment [21]. Few papers were interested on the study of the TCP-TiO_2 composites using hydroxyapatite and titania as starting materials [22–24]. In fact, titania has been added to the tricalcium phosphate matrix in the order of enhancing the mechanical performances of the TCP and not degrading its biocompatibility. Thereby, this study focused on the sintering and the mechanical properties of the tricalcium phosphate with different percentages of TiO_2 (2.5, 5, 7.5, 10, 20, 30, 40 and 50 wt%). In this study, the performances of the TCP-TiO_2 composites increase with the augmentation of the sintering temperature and the amount of titania. Thus, the best mechanical properties resulting from this study were obtained with the TCP-40 wt% TiO_2 composites after the sintering process at 1200°C for 1 h. The optimum values of the

TCP-40 wt% TiO_2 composites of mechanical strength, Vickers hardness, Young's and Shear modulus reached 33 MPa, 270 Hv, 33.1 GPa and 15.7 GPa, respectively. Thus, the aim of this study is to ameliorate the performances of the TCP-40 wt% TiO_2 composites by the inclusion of several additives to reach mechanical property similar to those of the bone tissues and precisely the enamel. Hence, MgF_2 has been chosen as a suitable compound for doping calcium phosphate [25]. Magnesium fluoride is an important material, which attracts attention thanks to its wide range of applications [26–32]. In the light of its technological properties, magnesium fluoride was studied in different area [26, 30, 33]. Among the alkaline-earth fluorides, MgF_2 crystallizes in the rutile-type structure [26, 27]. Thanks to the higher compressibility of MgF_2 and the relative sizes of its ions, the phase transformations of this material are found at lower pressures than those in many oxides [32]. The minor ions (Mg^{2+} and F^-) are incorporated in either the hydroxyapatite (HAp) or TCP crystal structure to replace the position of calcium, phosphorus or hydroxyl ion [25]. Fluoride is known to be important in suppressing dental caries [33, 34]. It stimulates the proliferation and the differentiation of bone cells [35]. The fluorine ion (F^-) has been investigated as an essential element for bone and dental formation in the human body [35, 36]. Fluoride compound is known as an effective additive for reducing the phase decomposition of hydroxyapatite due to the crystal structure stabilization [37]. Magnesium is an abundant and essential cation in the human body, since it has significant effects on human metabolism [38]. Mg^{2+} promotes the dental caries formation caused by the high calcification process in the bone formation [37, 38]. Even though, the lack of Mg^{2+} ion results from the inhibition of bone growth, the degradation of bone structure and the decrease of osteoblast adhesion [37, 38]. Evis and Pinar Sun [34] demonstrate the β-TCP structure stabilization and the hydroxyapatite formation by the heat treatment above 800°C. Hot pressed magnesium fluoride has been used as a dome material for many devices due to its excellent mechanical strength and thermal stability [39–41]. The study conducted by Kim et al. aimed to increase the mechanical properties and to inhibit the phase decomposition of HAp by the addition of MgF_2 in the HAp/ZrO_2 composites [37]. As a result, the MgF_2 (5 and 10 vol%) added to the HAp-zirconia composites completely suppresses the decomposition of hydroxyapatite into TCP below 1400°C owing to the ion substitution F^- for OH^- in the hydroxyapatite (HAp) crystal structure [37]. Many studies show that, the addition of MgF_2 to the tetragonal zirconia and HAp mixtures strongly reduces the tendency of HAp decomposition due to partial substitution of F^- for OH^- ions in the calcium phosphate structure [42, 43]. Therefore, MgF_2 enhances the tricalcium phosphate-titania composites performances by the inclusion of fluoride (F^-) and magnesium (Mg^{2+}) ions. On the other hand, fluoride presents the much more stable ion in acidic environment (pH = 4). This property is very important in medical fields and especially in dentistry [44]. According to the previous studies, fluoride has a great influence on the physical and biological properties of materials [45–47]. Additionally, fluoride is an essential trace element required for normal dental and skeletal development [47]. It has been shown that the presence of fluoride offers beneficial effects on increasing the quantity and quality of bone formation in the body [47, 48]. In the second time, we are interested in the examination of the effect of magnesium fluoride addition (1, 2.5, 3, 4, 4.5, 5, 6, 7.5 and 10 wt%) on the performances of the TCP-40 wt% TiO_2 composites sintered at 1200°C for different lengths of the sintering time. Then, we will characterize the resulting composites by different techniques such as Brazilian test (σ_r), Vickers indentation and ultrasonic technique, the magic angle scanning

nuclear magnetic resonance (^{31}P), the scanning electron microscopy, the infrared spectroscopy and the X-ray diffraction (XRD).

2. Materials and methods

The β-TCP powder resulted from a mixture of calcium carbonate ($CaCO_3$: Fluka, purity ≥ 98.5%) and calcium phosphate dibasic anhydrous ($CaHPO_4$: Fluka, purity ≥ 99%) after a heat treatment at 1000°C for 2 h according to the following reaction (Eq. (1))" [49]:

$$2CaHPO_4(s) + CaCO_3(s) \leftrightarrow Ca_3(PO_4) + H_2O + CO_2(g) \quad (1)$$

The initial powders used to obtain the TCP-TiO_2-MgF_2 composites were synthesized tricalcium phosphate (β-TCP), magnesium fluoride MgF_2 (Sigma Aldrich, purity > 98%) and titania TiO_2 (Fluka, purity > 98%). Firstly, Titania was introduced in the β-TCP matrix at different contents (2.5, 5, 7.5, 10, 20, 30, 40 and 50 wt%) followed by homogeneous mixing in a mortar. The heat treatment of the compacted disks was carried out in a vertical programmable muffle furnace (Pyrox 2408) at various temperatures (1000, 1100, 1200 and 1300°C) for 1 h. The theoretical density (d) was determined using the following Eq. (2):

$$d = (3.07A + 3.89B)/100 \quad (2)$$

where A and B are the weight ratios and 3.07 and 3.89 are the theoretical densities of β-TCP and anatase-TiO_2, respectively. The calculated theoretical densities of each composite are illustrated in **Table 1**.

Different amounts of MgF_2 (1, 2.5, 3, 4, 4.5, 5, 6, 7.5 and 10 wt%) were added to the TCP-40 wt% TiO_2 composites followed by homogeneous mixing in a mortar. The heat treatment of the compacted specimens was carried out in a vertical programmable muffle furnace (Pyrox 2408) at 1200°C for different sintering times. The theoretical density (d) was determined using the following Eq. (3):

A[a] (wt%)	B[a] (wt%)	d[b]
2.50	97.50	3.0905
5.00	95.00	3.1110
7.50	92.50	3.1315
10.00	90.00	3.1520
20.00	80.00	3.2340
30.00	70.00	3.3160
40.00	60.00	3.3980
50.00	50.00	3.4800

[a]A and B are the weight rates of TiO_2 and β-TCP, respectively.

[b]Theoretical density.

Table 1. The weight ratios of different TCP-TiO_2 composites.

$$d = (3.07\,A' + 3.89\,B' + 3.15\,C')/100 \quad (3)$$

where A′, B′ and C′ are the weight ratios and 3.07, 3.89 and 3.15 are the theoretical densities of β-TCP, anatase-TiO_2 and MgF_2, respectively. The calculated theoretical densities of all-composite are illustrated in **Table 2**.

The powders were mixed with absolute ethanol in an agate mortar. After milling these powders, the mixture was dried at 80°C for 24 h. After drying, the powder mixtures were molded in a cylinder with diameter 20 mm and thickness 4 mm and pressed under 150 MPa. The specimens were heated and cooled at rates of 10°C min^{-1} and 20°C min^{-1}, respectively.

The determination of the phase transformation in the microstructure of the elaborated composites was investigated by X-ray diffraction (XRD) analysis. The identification of the components phases was done by means Seifert XRD 3000 TT diffractometer with CuK_α radiation (λ = 1.54056 Å). The phase identification was operated resulting from the comparison between experimental XRD patterns and standards files compiled by the International Center for Diffraction Data (ICDD). The powders were then characterized by infrared spectrometric analysis with attenuated total reflection method (ATR) (Agilent Cary 630 Fourier Transform Infrared Spectrometer (FTIR)). The powders were submitted to the ^{31}P magic angle scanning nuclear magnetic resonance (MAS-NMR) on a Brucker 300 WB spectrometer.

The microstructure of the fractured surfaces of the sintered samples was investigated with scanning electron microscope (SEM) (JEOL JSM 5800LV) after enhancing their conductivity with a gold layer.

The powder's size was measured through a Micromeritics Sedigraph 5000. The specific surface area (SSA) was determined by the BET method with azote (N_2) as the adsorbed gas (ASAP 2010) [50].

A′[a] (wt%)	B′[a] (wt%)	C′[a] (wt%)	d[b]
59.50	39.50	1.00	3.3947
58.75	38.75	2.50	3.3897
58.50	38.50	3.00	3.3881
58.00	38.00	4.00	3.3848
57.75	37.75	4.50	3.3831
57.50	37.50	5.00	3.3815
57.00	37.00	6.00	3.3782
56.25	36.25	7.50	3.3732
55.00	35.00	10.00	3.3650

[a]A′, B′ and C′ are the weight rates of β-TCP, TiO_2 and MgF_2, respectively.
bTheoretical density.

Table 2. The weight ratios of the different TCP-TiO_2-MgF_2 composites.

The main particle size (D_{BET}) was calculated by assuming that the primary particles are spherical (Eq. (4)) [51]:

$$D_{BET} = \frac{6}{S\rho} \tag{4}$$

where ρ is the theoretical density and S is the surface specific area.

The densification of the sintered specimens was evaluated by the measurements of the specimen dimensions. The relative error of the densification value was about 1%.

Thermal expansion-shrinkage of the compact powder was measured with a dilatometer (Model Setaram TMA 92 dilatometer). About 20 mg of powder was heated with a heating rate of 10°C min^{-1} along with alumina as a reference material and a low stream of argon gas. The heating and cooling rates were 10 and 20°C min^{-1}, respectively.

The Brazilian test was used to measure the mechanical strength of the samples [52, 53]. The rupture strength (σ_r) (or mechanical strength) was calculated based on the maximum applied load recorded (P) and sample's dimensions (D being the diameter and t being the thickness) using (Eq. (5)):

$$\sigma_r = \frac{2 \times P}{\pi \times D \times t} \tag{5}$$

The sintered samples were examined by Vickers test indentation using loading values of 49 or 98 N applied for 15 s. This test was investigated after polishment of the samples surfaces between 1 and 3 μm with diamond paste. Vickers hardness value (H) was determined by Eq. (6) [54]:

$$H = 1.854(P/d^2) \tag{6}$$

where H is Vickers hardness, 'd' is the indent diagonal length and P is the indentation load.

The characterization of the samples using ultrasound technique promotes the determination of both Young's and Shear moduli value [55]. The measurement was done by a high-frequency generator Model 5077PR (Olympus). Young's modulus and the Shear modulus were calculated from the point of the longitudinal and the transversal ultrasonic velocities [55].

3. Results

3.1. Characterization of the starting powders

Table 3 presents the particles size distribution data (measured by granulometric repartition), the SSA and the calculated average grain sizes (D_{BET}) of the β-TCP, TiO_2 and MgF_2 powders. The averages of the grain's size of the samples obtained through the SSA (D_{BET}) and the granulometric repartition (D_{50}) are different. This difference may be due to the presence of agglomerates in the initial powders (**Table 3**).

The curve of the differential thermal analysis of the β-TCP shows the presence of two endothermic peaks: the first large band located between 1230 and 1270°C is attributed to the first allotropic transformation of the tricalcium phosphate (β–α) and the second peak registered

at 1470°C is relative to the second transformation of TCP (α–α') (**Figure 1a**). These results are mentioned in previous works from literature [12, 56]. The Differential thermal analysis (DTA) curve of the TiO_2 shows that no evolution can be obtained with the sintering temperature (**Figure 1b**). The thermogram of the TCP-10 wt% TiO_2 composites reveals the appearance of two endothermic peaks (**Figure 1c**). The first peak at 1470°C is attributed to the second transformation of the β-TCP (α–α') while the new peak at 1440°C is probably relative to the

Compounds	SSA (m^2/g)	D_{BET} (μm)	D_{50} [a] (μm)	d[b]
TiO_2	12.00	0.11	0.20	3.89
β-TCP	0.80	2.80	6.00	3.07
MgF_2	37.00	0.05	0.10	3.15

[a]Mean diameter.
[b]Theoretical density.

Table 3. Characteristics of the different powders used in the study.

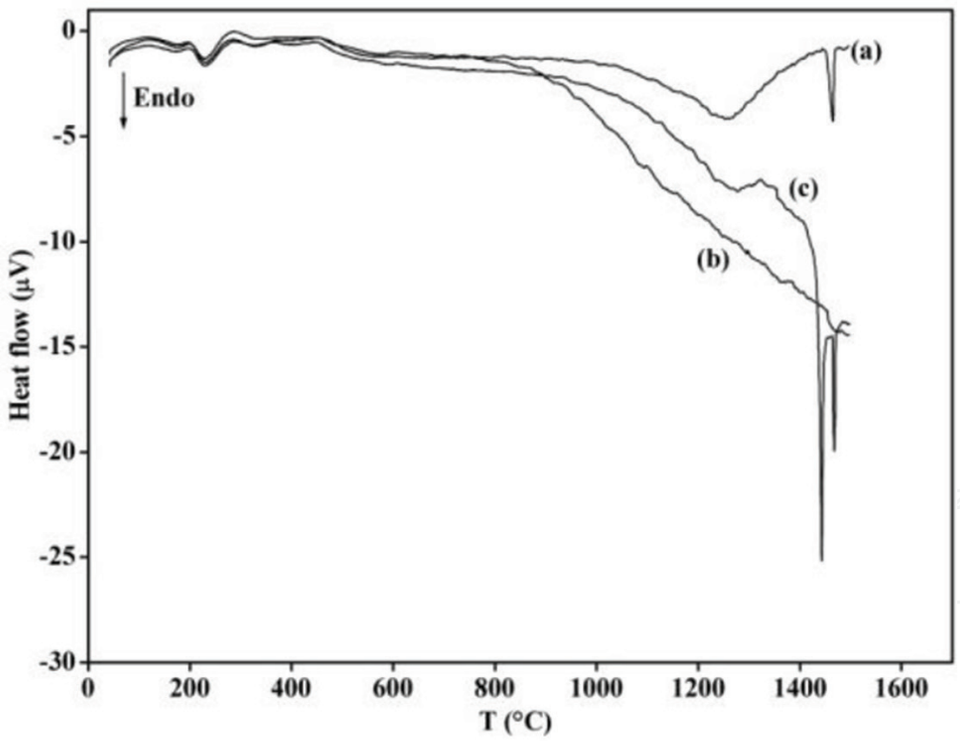

Figure 1. DTA curves of: (a) β-TCP, (b) anatase-TiO_2 and (c) TCP-10 wt% TiO_2 composites.

liquid phase formation. Furthermore, the melting points of both β-TCP and TiO_2 are 1756 and 1855°C, respectively [22]. Thus, the liquid phase is formed between TiO_2 and β-TCP, and it is not relative to the melting point of the initial powders. The results are similar to that found in the previous studies [12, 22]. They show that in the TiO_2/β-TCP system, there is an

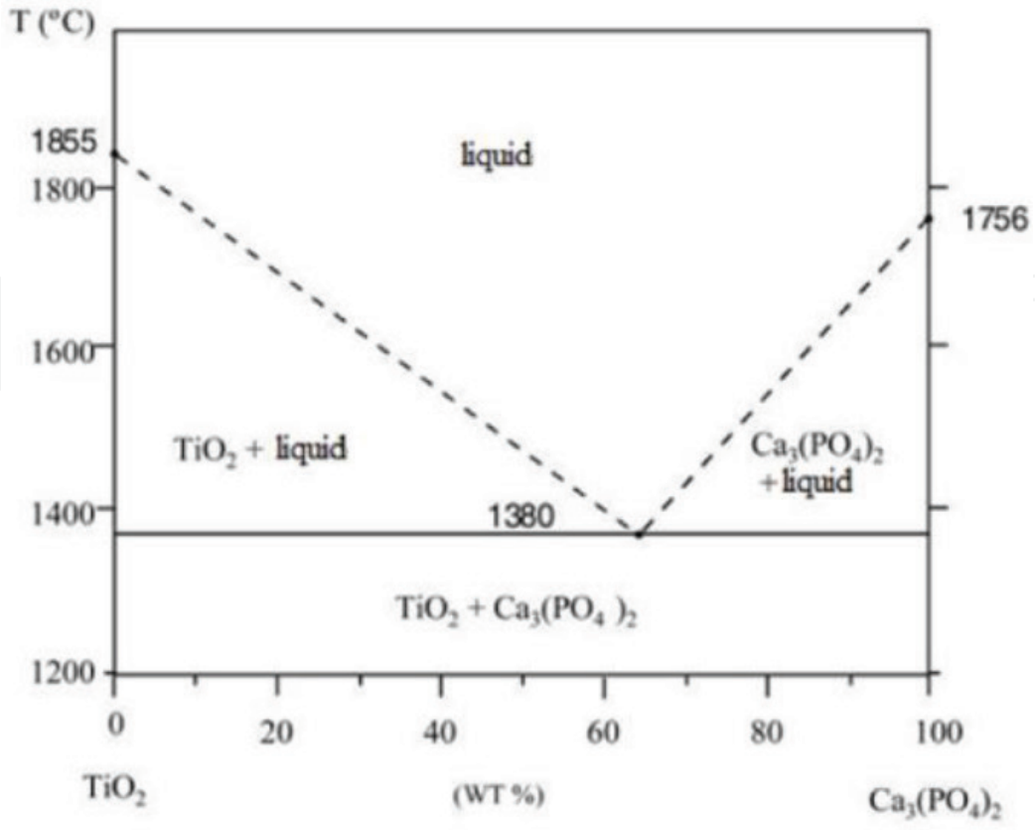

Figure 2. Phase equilibrium diagram of the TiO_2-$Ca_3(PO_4)_2$ system [22].

eutectic with a composition of 63 wt% TCP-37 wt% TiO_2 at 1380°C [22]. **Figure 2** confirms the presence of the liquid phase which is showed in the binary diagram of the $Ca_3(PO_4)_2$/TiO_2 [22].

Figure 3 shows the dilatometric measurements of different powders used in this study (β-TCP, TiO_2, TCP-10 wt% TiO_2 composites and MgF_2). The sintering temperature of the initial powder began at about 1000, 900 and 800°C for the β-TCP, the TiO_2 and the MgF_2, respectively (**Figure 3a–c**). The peak at 1230°C is attributed to the first allotropic transformation of the tricalcium phosphate (**Figure 3a**). The shrinkage curve of the titania powder reveals one peak which is relative to the phase transformation from anatase to rutile at 1090°C (**Figure 3b**). This result was well-confirmed by literature [57]. In fact, they showed that the commercial anatase-titania powder has been transformed into the rutile structure at about 1000°C [57], which confirms our results. The curve of the pure MgF_2 indicates that the shrinkage was manifested at 800°C until 1150°C (**Figure 3c**). In fact, the rate of maximum densification corresponds to the inflection point, which is obtained at 890°C (**Figure 3c**). **Figure 3d** presents the shrinkage curve of the TCP-10 wt% TiO_2 composites. In fact, no evolution was reported with the TCP-10 wt% TiO_2 composites (**Figure 3d**). As a result, the content of 10 wt% TiO_2 stabilizes the TCP structure and prevents the inverse allotropic transformation of TCP from the α phase to the β phase. The stabilization was well-explained by the exchange of Ca^{2+} and Ti^{4+} ions derived from β-TCP and TiO_2.

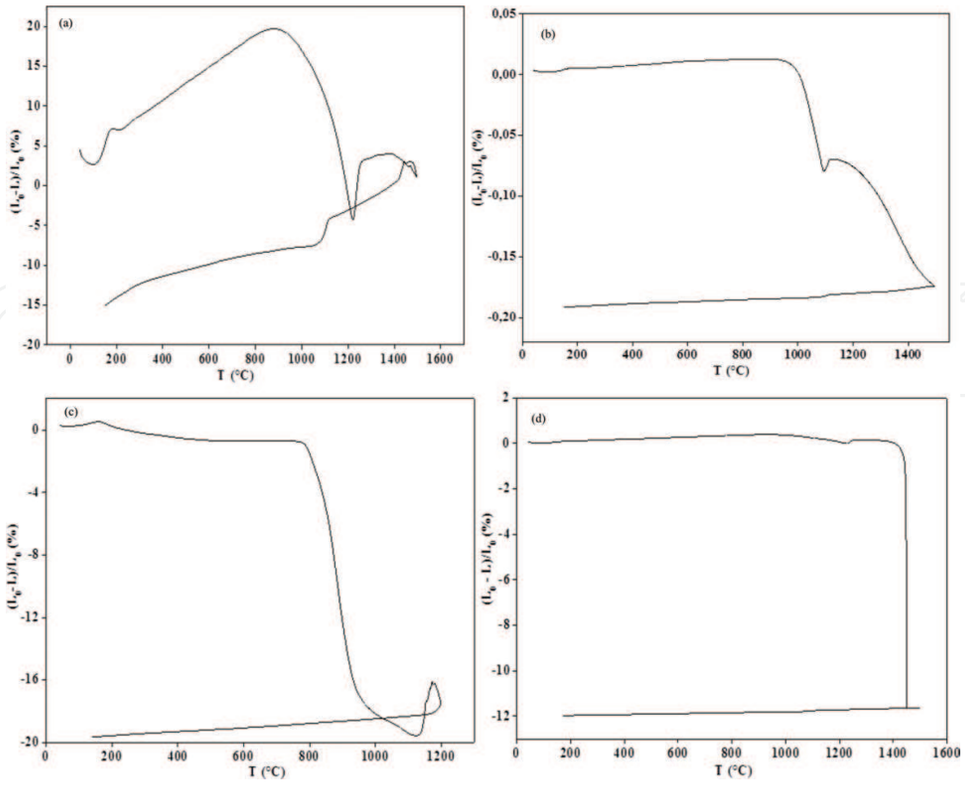

Figure 3. Linear shrinkage curves of: (a) β-TCP, (b) TiO_2, (c) MgF_2 and (d) TCP-10 wt% TiO_2 composites.

3.2. Effect of the addition of titania on the densification and the mechanical properties of the tricalcium phosphate

The evolution of the densification of the tricalcium phosphate was studied with the addition of titania between 1000 and 1300°C. **Figure 4** shows the typical relationship between temperature and density. The density of the β-TCP sintered with different percentages of the TiO_2 (2.5, 5, 7.5, 10, 20, 30, 40 and 50 wt%) increases with the sintering temperature (**Figure 4**). At 1200°C, the optimum value of the densification (89%) was obtained with 40 wt% TiO_2 (**Figure 4g**). Above 1200°C, the performances of the composites decrease abruptly (**Figure 4**).

Figure 5 shows the influence of the titania additive (2.5, 5, 7.5, 10, 20, 30, 40 and 50 wt%) at various sintering temperatures (1000, 1100, 1200 and 1300°C) on the rupture strength of TCP. The mechanical strength of the TCP-TiO_2 composites improves with both the content of TiO_2 and the sintering temperature (**Figure 5**). At 1200°C, the rupture strength of the TCP-40 wt% TiO_2 composites reached its maximum value (33 MPa) (**Figure 5g**). Above 1200°C, the rupture strength of the TCP-TiO_2 composites was hindered abruptly (**Figure 5**). The discrepancy of results appears especially after the addition of 50 wt% TiO_2 in the tricalcium phosphate matrix (**Figure 5h**). The amelioration of these performances of the TCP-40 wt% TiO_2 composites could be according to the formation of a liquid phase between TiO_2 and β-TCP.

The evolution of Vickers hardness with different percentages of titania at various temperatures was shown in **Figure 6**. Vickers hardness reached its optimum value (270 Hv) at 1200°C with 40 wt% TiO_2. Then, Vickers hardness value decreases with the sintering temperature.

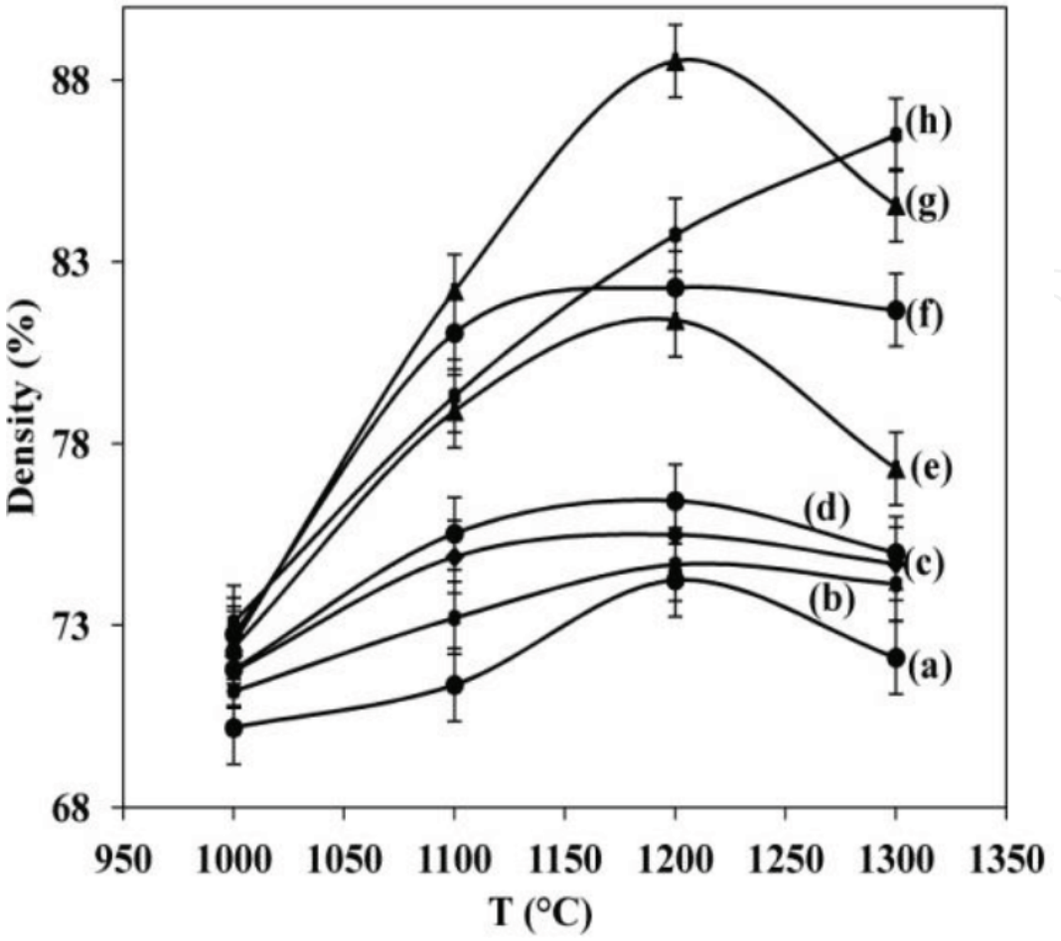

Figure 4. Relative density versus temperature of the β-TCP sintered for 1 h with different percentages of TiO_2: (a) 2.5 wt%, (b) 5 wt%, (c) 7.5 wt%, (d) 10 wt%, (e) 20 wt%, (f) 30 wt%, (g) 40 wt% and (h) 50 wt%.

Figures 7 and **8** present the evolution of elastics moduli (E and G) of the β-TCP sintered with different contents of TiO_2 (2.5, 5, 7.5, 10, 20, 30, 40 and 50 wt%) at various temperatures (1000, 1100, 1200 and 1300°C). The optimum values of both Young's modulus and Shear modulus reached 33.1 and 15.7 GPa, respectively, with 40 wt% TiO_2. Beyond 40 wt% TiO_2, the properties of the composites were hold up with the increase of the sintering temperature (**Figures 7** and **8**).

3.3. Effect of the magnesium fluoride addition on the densification and the mechanical properties of the tricalcium phosphate-titania composites

The effect of the magnesium fluoride addition on the performances of the TCP-40 wt% TiO_2 composites has been assessed by the measurement of the density and the rupture strength. The densification behavior of the TCP-40 wt% TiO_2 composites sintered at 1200°C for 1 h with different amounts of MgF_2 (1, 2.5, 3, 4, 4.5, 5, 6, 7.5 and 10 wt%) is reported in **Figure 9**. These results show a significant improvement of the relative density of the TCP-TiO_2 composites as a function of the magnesium fluoride added (**Figure 9**). The density of the TCP-TiO_2 composites increases from 3 wt% MgF_2 and remains constant until 6 wt%

http://dx.doi.org/10.5772/intechopen.68501

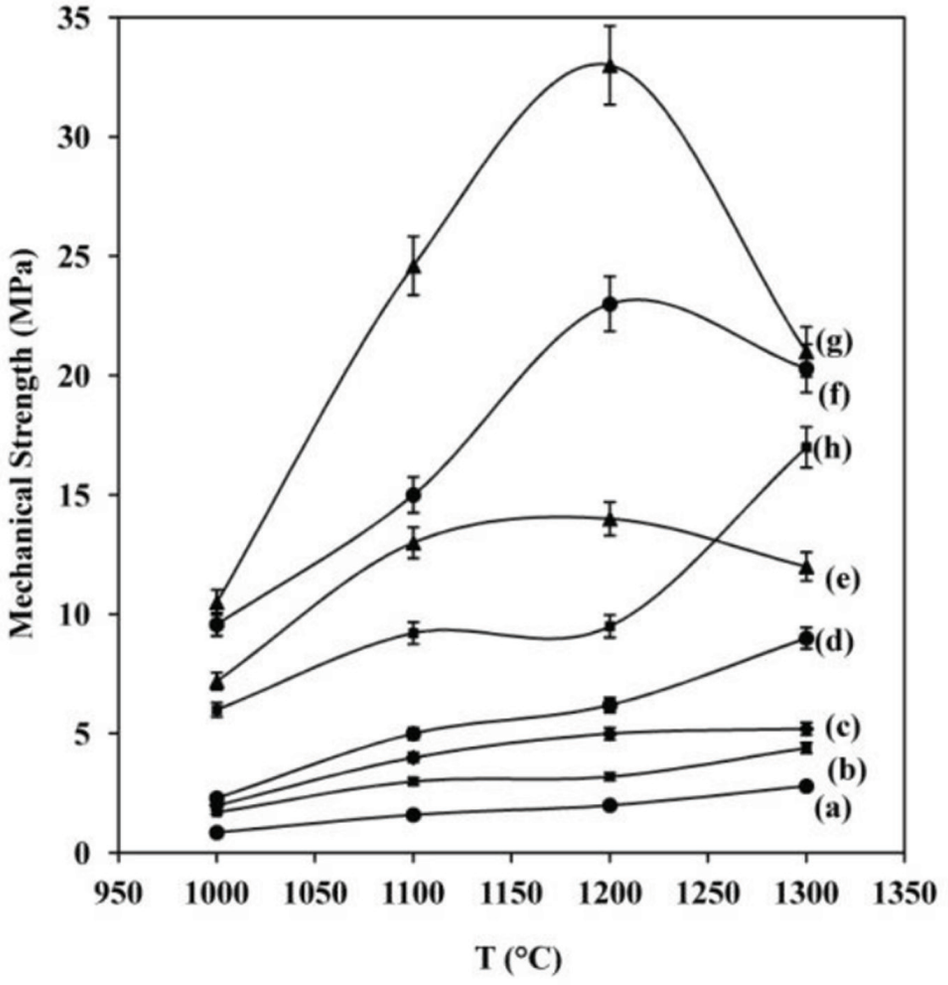

Figure 5. Mechanical strength versus temperature of the β-TCP sintered for 1 h with different percentages of TiO_2: (a) 2.5 wt%, (b) 5 wt%, (c) 7.5 wt%, (d) 10 wt%, (e) 20 wt%, (f) 30 wt%, (g) 40 wt% and (h) 50 wt%.

MgF_2, then the density of the composites decreases abruptly (**Figure 9**). The optimum value of the densification was about 94% with 4 wt% MgF_2. This result is obviously close to the full densification.

Figure 10 shows the rupture strength of the TCP-40 wt% TiO_2 composites sintered at 1200°C for 1 h with different percentages of MgF_2 (1, 2.5, 3, 4, 4.5, 5, 6, 7.5 and 10 wt%). Thus, the rupture strength reached its maximum value (27 MPa) after the addition of 4 wt% MgF_2 (**Figure 10**). Above 4 wt% MgF_2, the rupture strength decreases sharply (**Figure 10**). A remarkable amelioration of the rupture strength of the TCP-40 wt% TiO_2 composites was obtained with 10 wt% MgF_2 (**Figure 10**).

The influence of the magnesium fluoride addition on Vickers hardness was studied at 1200°C with the same percentages of MgF_2 (**Figure 11**). The addition of MgF_2 outstandingly enhanced Vickers hardness of the TCP-40 wt% TiO_2 composites (**Figure 11**). Thus, the incorporation of 4 wt% of MgF_2 to the composites led to a maximum of Vickers hardness (360 Hv) after the

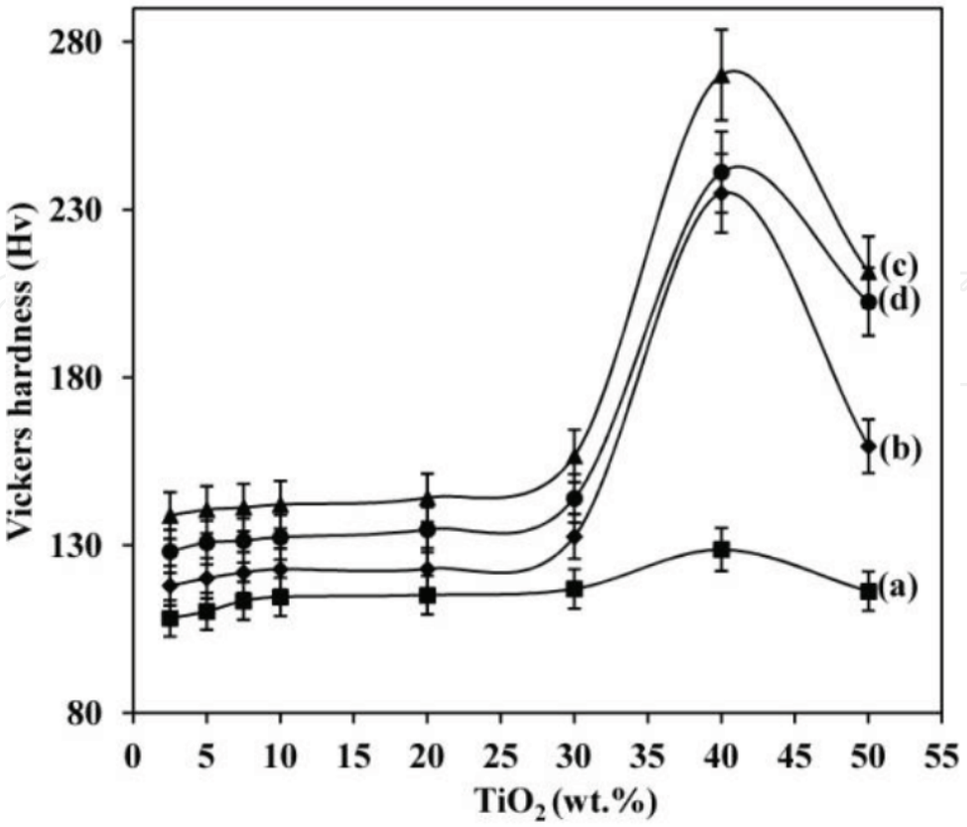

Figure 6. Vickers hardness versus temperature of the β-TCP sintered for 1 h with different percentages of TiO_2 at: (a) 1000°C; (b) 1100°C; (c) 1200°C and (d) 1300°C.

sintering process at 1200°C for 1 h. Beyond 4 wt% MgF_2, Vickers hardness of the composites was hindered (**Figure 11**). However, Vickers hardness of the TCP-40 wt% TiO_2 composites increases slowly with 10 wt% MgF_2 (**Figure 11**).

The evolution of the elastic modulus (E and G) of the TCP-40 wt% TiO_2 composites sintered with different contents of MgF_2 is shown in **Figure 12A** and **B**, respectively. The elastic modulus of the TCP-40 wt% TiO_2 composites increase with the addition of MgF_2 (**Figure 12A** and **B**). Thus, the optimum values of Young's modulus and the Shear modulus of the TCP-40 wt% TiO_2 composites are obtained by adding 4 wt% MgF_2 and these values reach 51 and 20 GPa, respectively. The performances of the samples were hindered with the increase of the percentages of MgF_2 in the TCP-40 wt% TiO_2 composites (**Figure 12A** and **B**).

Figure 13 illustrates a typical relation between the different lengths of the sintering time and the densification of the TCP-38 wt% TiO_2-4 wt% MgF_2 composites after the sintering temperature at 1200°C. The maximum value of densification (94%) was registered after the sintering process at 1200°C for 1 h (**Figure 13**). The densification's value decreases with the sintering time (**Figure 13**).

Figure 14 depicts the rupture strength evolution of the samples after the sintering process at 1200°C for different length of the sintering time. The mechanical strength of the TCP-TiO_2-MgF_2

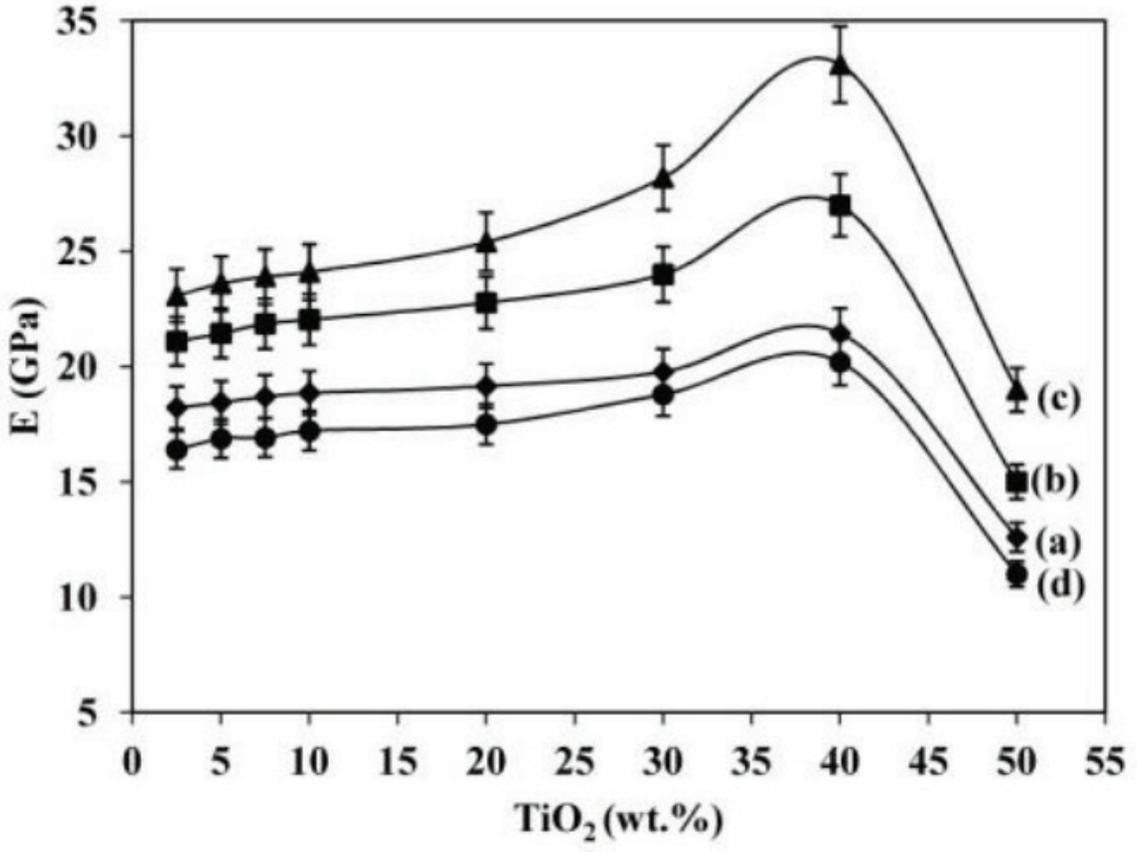

Figure 7. Young's modulus of the β-TCP sintered for 1 h with different percentages of TiO_2 at: (a) 1000°C; (b) 1100°C, (c) 1200°C and (d) 1300°C.

composites was enhanced after the sintering process at 1200°C for 1 h and reached 27 MPa then, decreases abruptly (**Figure 14**). This amelioration was associated to the important densification (**Figures 13** and **14**).

Figure 15 shows the evolution of Vickers hardness of the TCP-38 wt% TiO_2-4 wt% MgF_2 composites with the length of the sintering time. Vickers hardness increases and reaches its optimum value (360 Hv) for 1 h (**Figure 15**). Then, a remarkable diminution of Vickers hardness of the samples was registered above 1 h (**Figure 15**).

The evolution of the elastic moduli (E and G) of the TCP-38 wt% TiO_2-4 wt% MgF_2 composites sintered for different length of the sintering time at 1200°C is pictured in **Figure 16A** and **B**, respectively. The sintering time has no effect on the elastic moduli (**Figure 16A** and **B**). Young's modulus reached 51 GPa as maximum value while Shear modulus reached 20 GPa as an optimum value (**Figure 16A** and **B**).

3.4. Characterization of the TCP-TiO_2-MgF_2 composites

After the sintering process, the samples were investigated by different characterization techniques such as: XRD, IR, ^{31}P MAS-NMR and SEM.

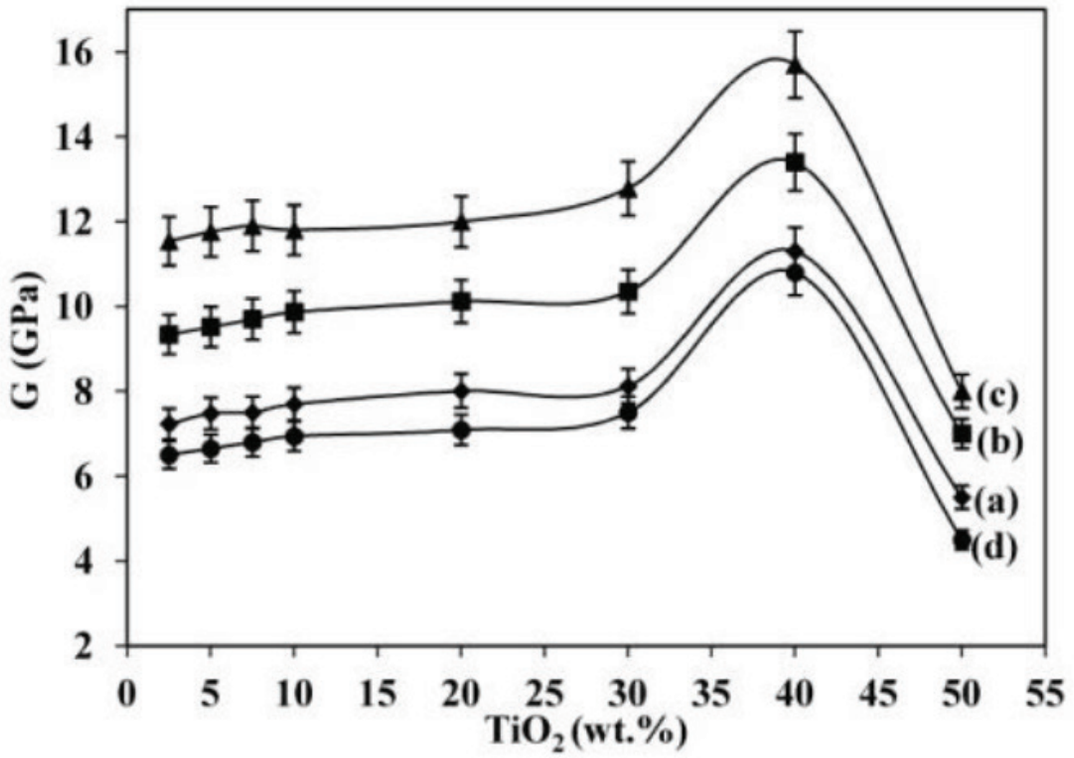

Figure 8. Shear modulus of the β-TCP sintered for 1 h with different percentages of TiO_2 at: (a) 1000°C, (b) 1100°C, (c) 1200°C and (d) 1300°C.

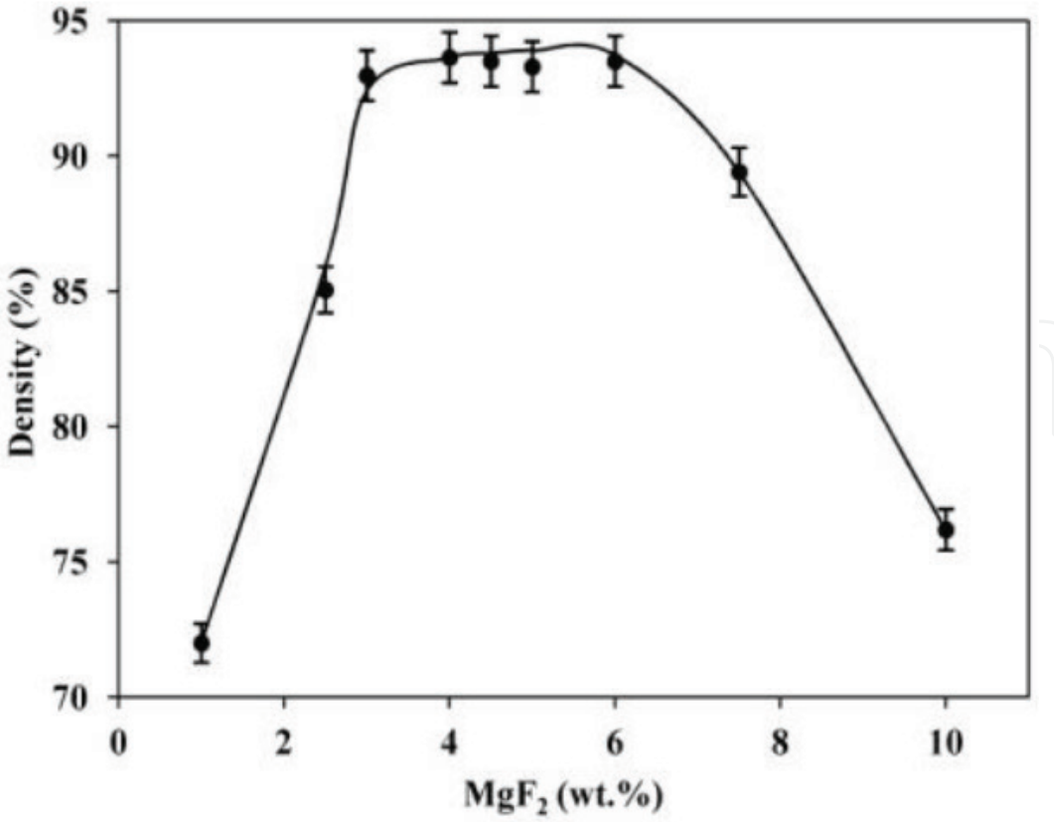

Figure 9. Relative density of the TCP-40 wt% TiO_2 composites sintered at 1200°C for 1 h with different percentages of MgF_2.

http://dx.doi.org/10.5772/intechopen.68501

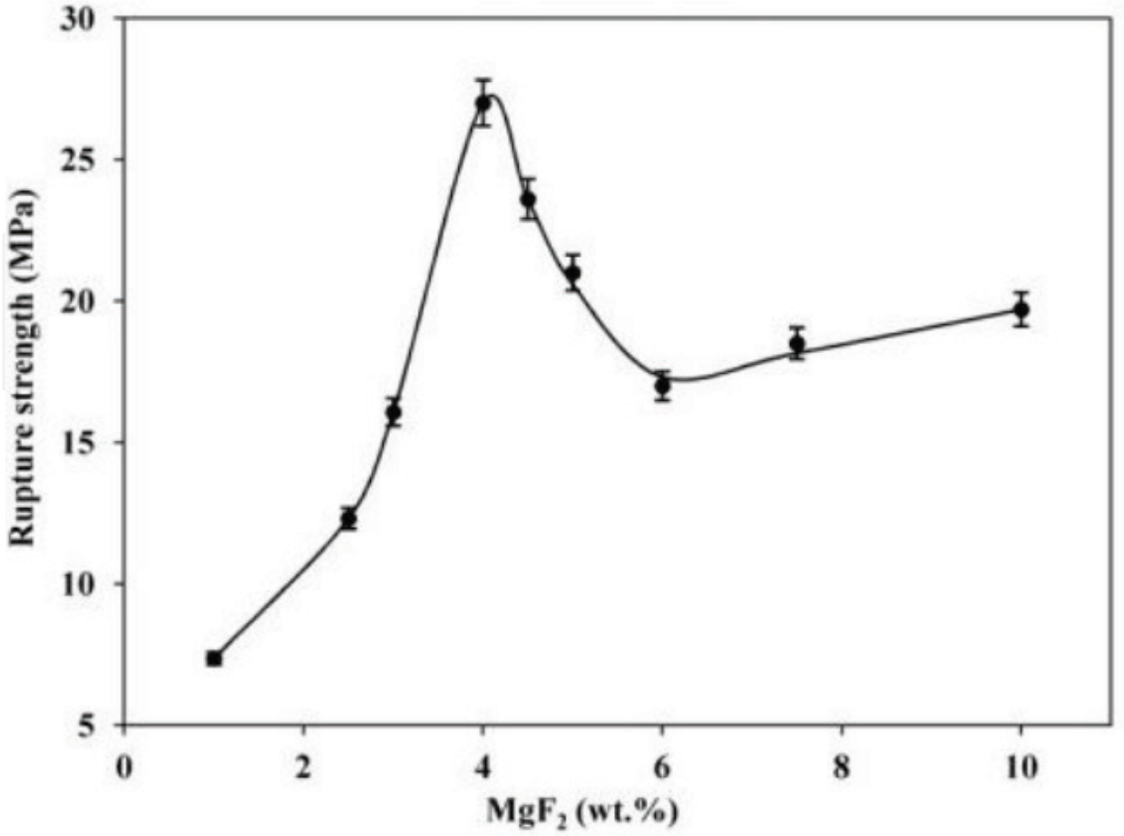

Figure 10. Rupture strength of the TCP-40 wt% TiO_2 composites sintered at 1200°C for 1 h with different percentages of MgF_2.

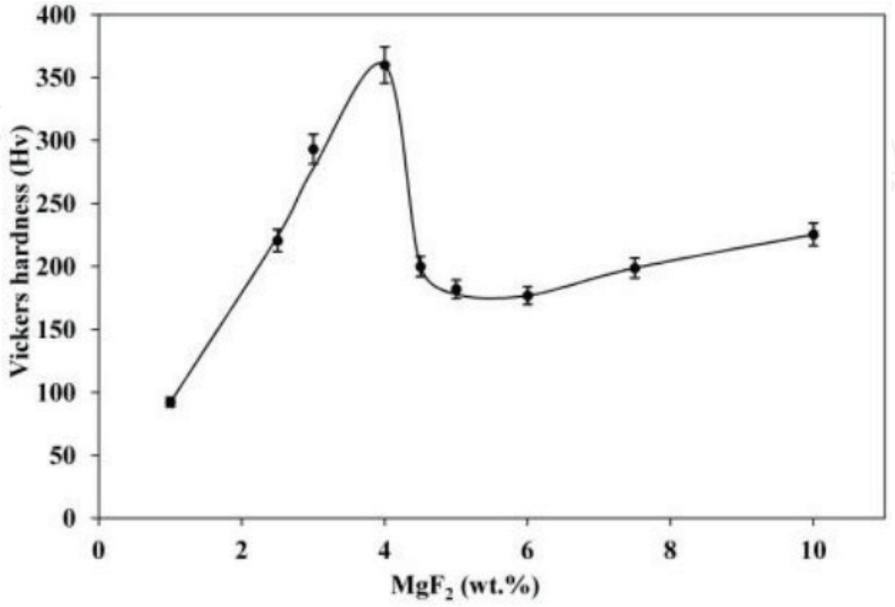

Figure 11. Vickers hardness of the TCP-40 wt% TiO_2 composites sintered at 1200°C for 1 h with different percentages of MgF_2.

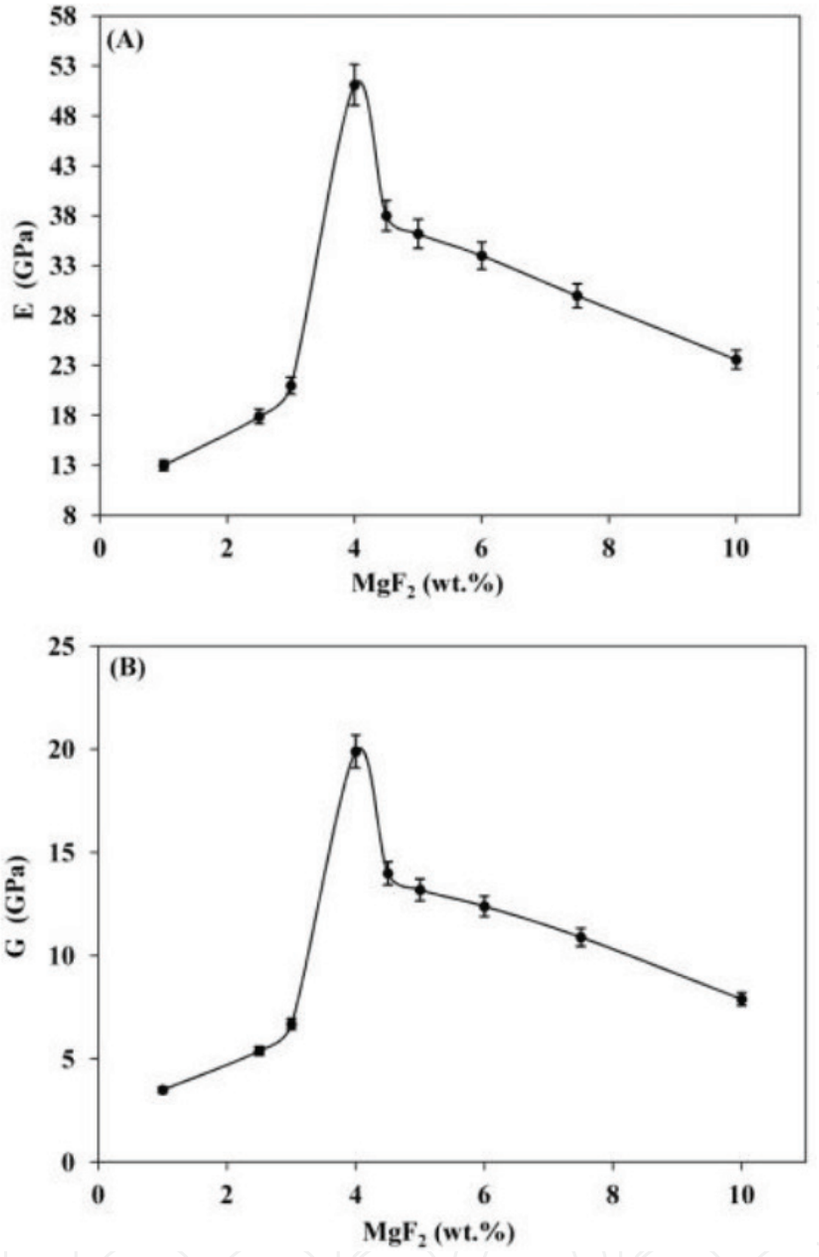

Figure 12. Elastic modulus of the TCP-40 wt% TiO_2 composites sintered at 1200°C for 1 h with different percentages of MgF_2: (A) Young's modulus and (B) the Shear modulus.

Figure 17 shows the XRD patterns of the samples sintered at 1200°C for 1 h without and with different contents of MgF_2 (1, 2.5, 4, 4.5, 5, 7.5 and 10 wt%). The diffraction pattern of the TCP-40 wt% TiO_2 composites sintered without MgF_2 displays the α-TCP phase traces presence (ICDD data file no. 43-1484), the calcium titanate ($CaTiO_3$) (ICDD data file no. 89-8033), the β-TCP phase (ICDD data file no. 70-2065) and the rutile phase of titania (ICDD data file no. 65-1119) (**Figure 17a**). The introduction of 1 wt% MgF_2 to the TCP-40 wt% TiO_2 led to the presence of traces of both calcium titanate ($CaTiO_3$) and fluorapatite (FAp) (ICDD data file no. 76-0558) beside the β-TCP phase and the rutile phase of titania in majority peaks (**Figure 17b**). Further increasing the percentage of MgF_2 to the TCP-TiO_2 composites, we

http://dx.doi.org/10.5772/intechopen.68501

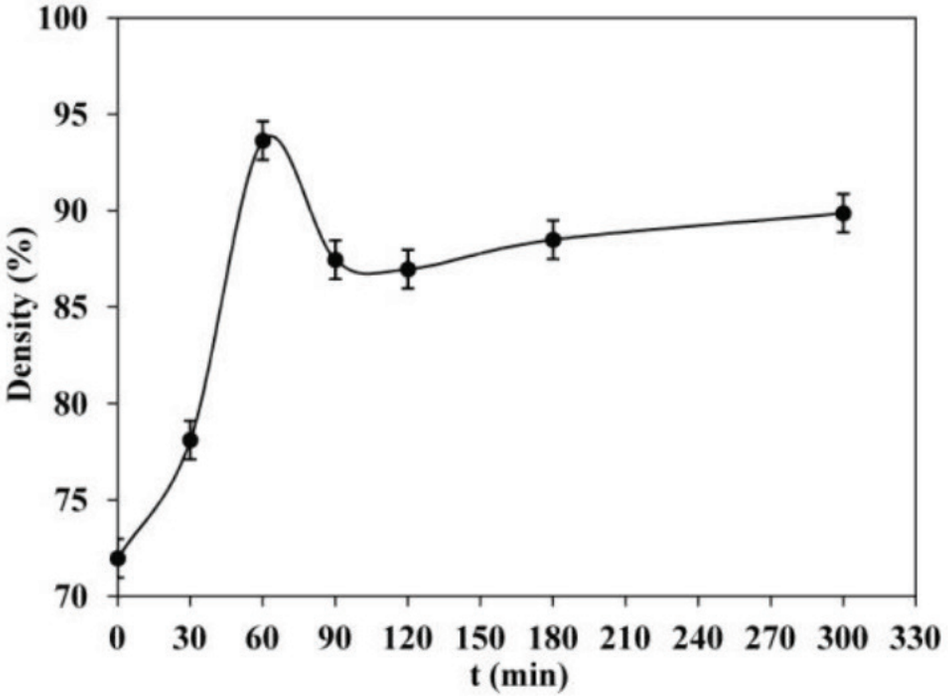

Figure 13. Relative density of the TCP-38 wt% TiO_2-4 wt% MgF_2 composites sintered at 1200°C for different length of the sintering time.

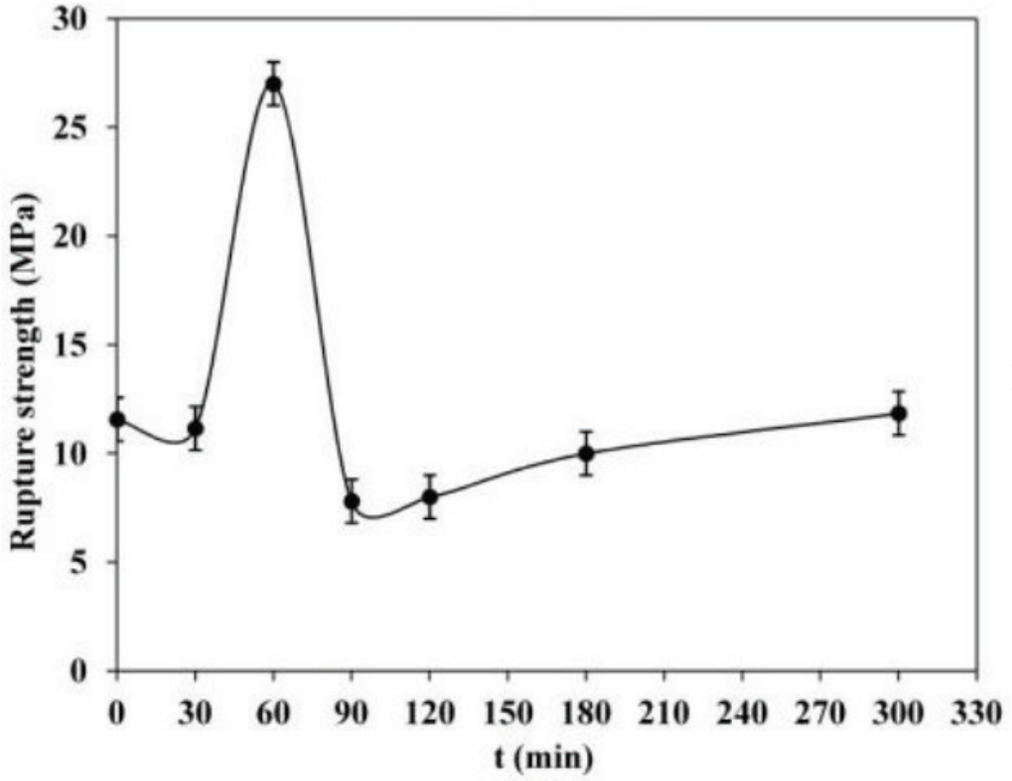

Figure 14. Rupture strength of the TCP-38 wt% TiO_2-4 wt% MgF_2 composites sintered at 1200°C for different length of the sintering time.

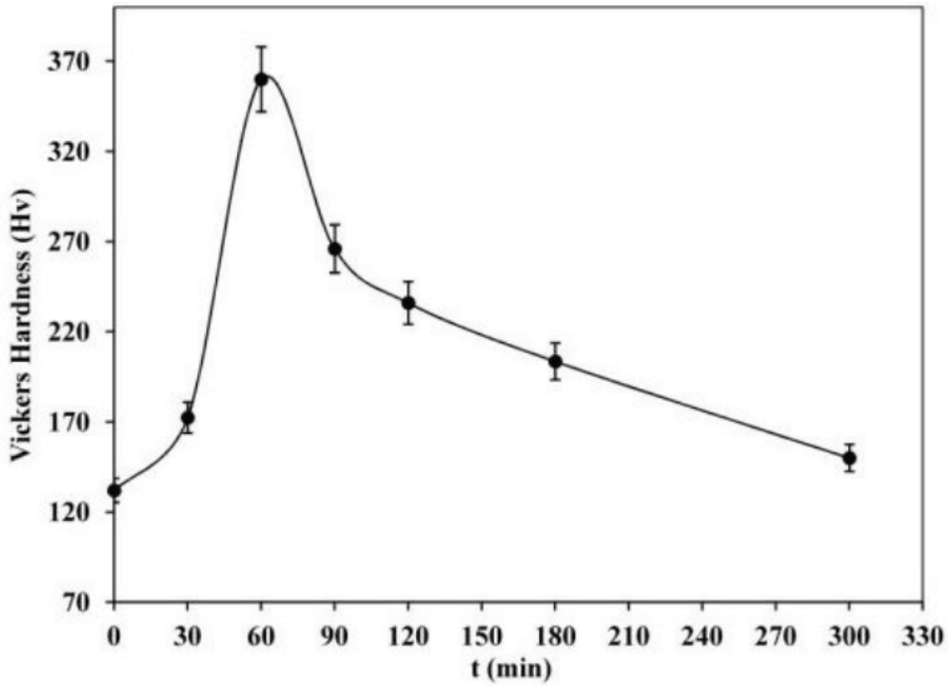

Figure 15. Vickers hardness of the TCP-38 wt% TiO_2-4 wt% MgF_2 composites sintered at 1200°C for different length of the sintering time.

obtain more of fluorapatite (**Figure 17b–h**). Nevertheless, the β-TCP phase is disappeared and the rutile phase quite occupied the majority of peaks (**Figure 17c–h**). The appearance of a new phase relative to $Mg_2(PO_4)F$ (ICDD data file no. 42-0582) was detected after the addition of 2.5, 4 and 4.5 wt% MgF_2 (**Figure 17c–e**). At higher contents of MgF_2 (after 4.5 wt%), the $Mg_2(PO_4)F$ phase is completely disappeared and the intensity of fluorapatite increased (**Figure 17f–h**).

Figure 18 displays the FTIR spectra of the TCP-40 wt% TiO_2 composites sintered at 1200°C for 1 h without and with different percentages of MgF_2 (1, 2.5, 4, 4.5, 5, 7.5 and 10 wt%). Most bands characterize the phosphate group of calcium phosphate (**Figure 18**). Therefore, the bands at 954 and 965 cm^{-1} are assigned to the symmetric stretching of the PO_4^3 ions while the bands at 1033 and 1093 cm^{-1} are relative to the asymmetric stretching of the PO_4^3 ions (**Figure 18**).

The ^{31}P MAS-NMR spectra of the TCP-40 wt% TiO_2 composites sintered at 1200°C for 1 h without and with different amounts of MgF_2 (1, 2.5, 4, 4.5, 5, 7.5 and 10 wt%) are illustrated in **Figure 19**. This analysis indicates the presence of the tetrahedral environment, which is assigned to the resonance characteristic of the phosphate group (**Figure 19**). Moreover, the ^{31}P MAS-NMR spectrum of the TCP-40 wt% TiO_2 composites sintered without MgF_2 shows many tetrahedral environments: one broad peak centered at 4 ppm, a shoulder at 0.47 ppm and an intense peak at −0.62 ppm (**Figure 19a**). The NMR spectrum of the TCP-40 wt% TiO_2-1 wt% MgF_2 composites presents an allure modification (**Figure 19b**). One intense peak located at 3 ppm is probably attributed to the phosphor of the phosphate groups of the FAp (**Figure 19c–h**). The second peak at 0.6 ppm is probably relative to the phosphor of the phosphate groups of the

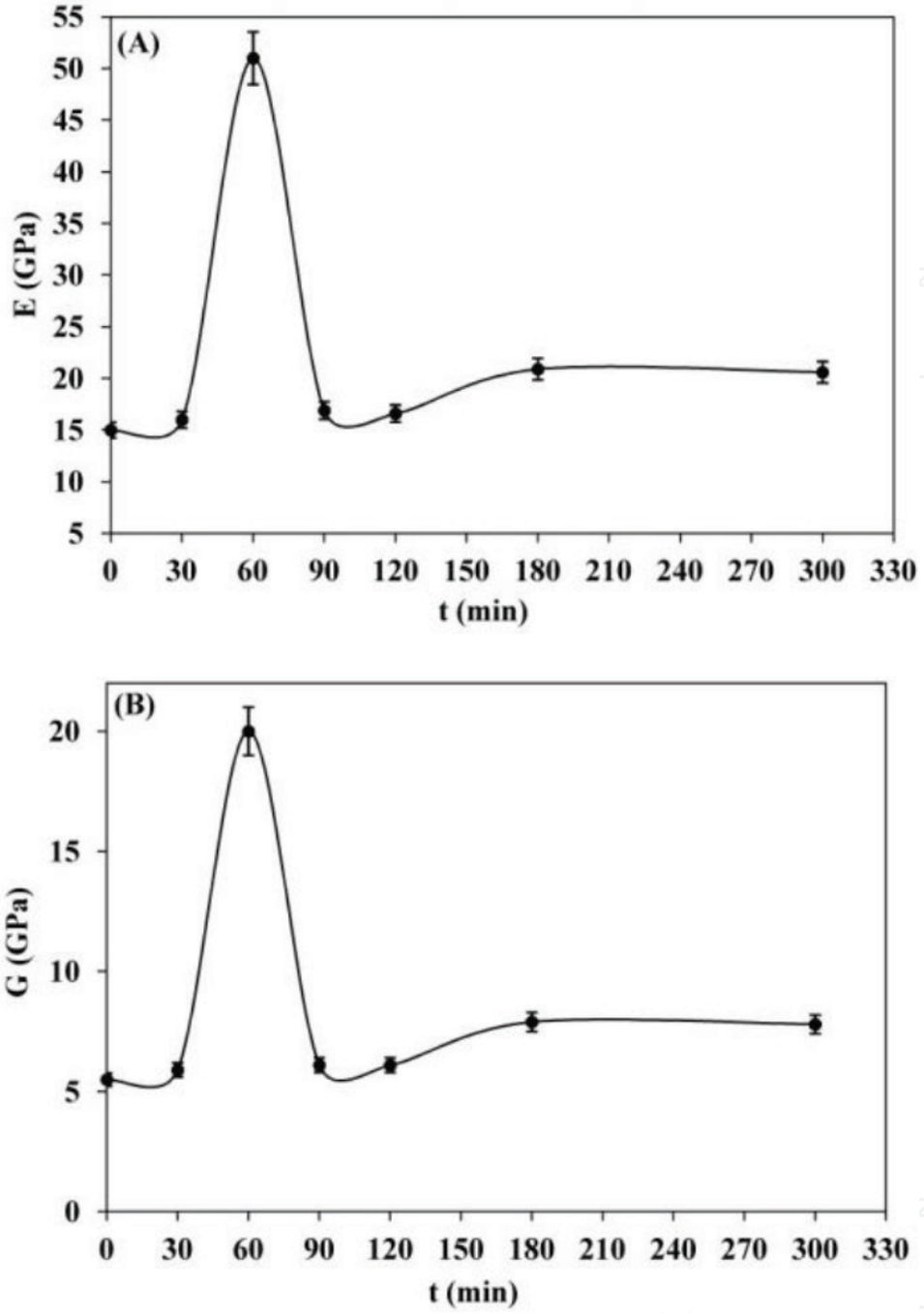

Figure 16. Elastic modulus of the TCP-38 wt% TiO_2-4 wt% MgF_2 composites sintered at 1200°C for different length of the sintering time: (A) Young's modulus and (B) the Shear modulus.

$Mg_2(PO_4)F$ (**Figure 19b–e**). The intensity of the first peak increases with the amount of MgF_2 while the intensity of the second peak decreases and disappears with the TCP-40 wt% TiO_2-4.5 wt% MgF_2 composites (**Figure 19f–h**).

The microstructure of the sintered samples was observed using the SEM analysis. **Figure 20** shows the micrographs of the TCP-40 wt% TiO_2 composites sintered at 1200°C for 1 h

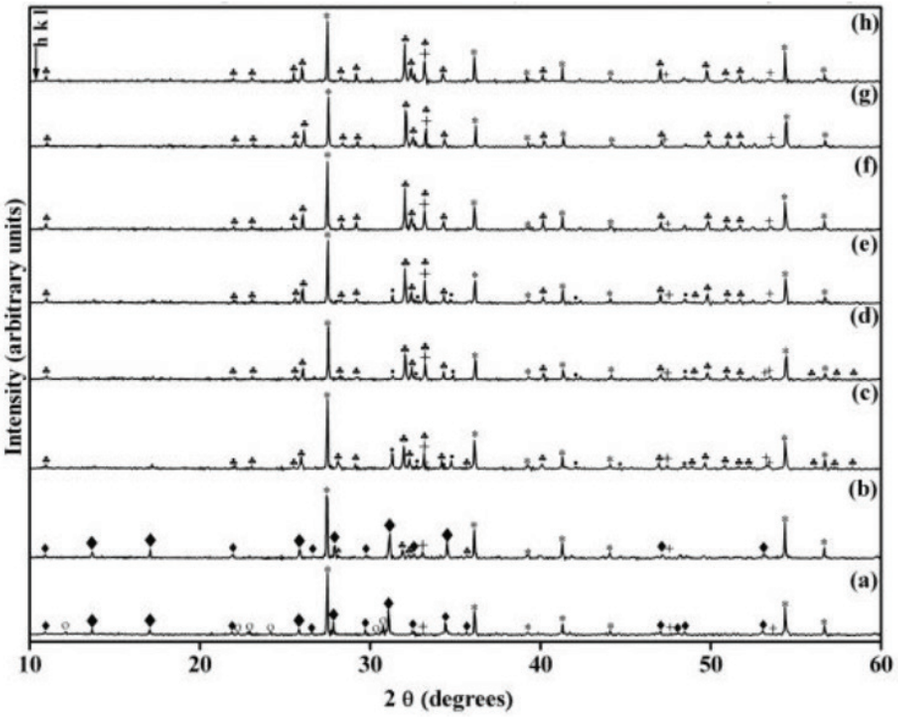

Figure 17. XRD patterns of the TCP-40 wt% TiO_2 composites sintered at 1200°C for 1 h without and with different percentages of MgF_2: (a) 0 wt%, (b) 1 wt%, (c) 2.5 wt%, (d) 4 wt%, (e) 4.5 wt%, (f) 5 wt%, (g) 7.5 wt% and (h) 10 wt%. (o: α-TCP, ♦: β-TCP, +: $CaTiO_3$, *: rutile, ♣: fluorapatite, ●: $Mg_2(PO_4)F$).

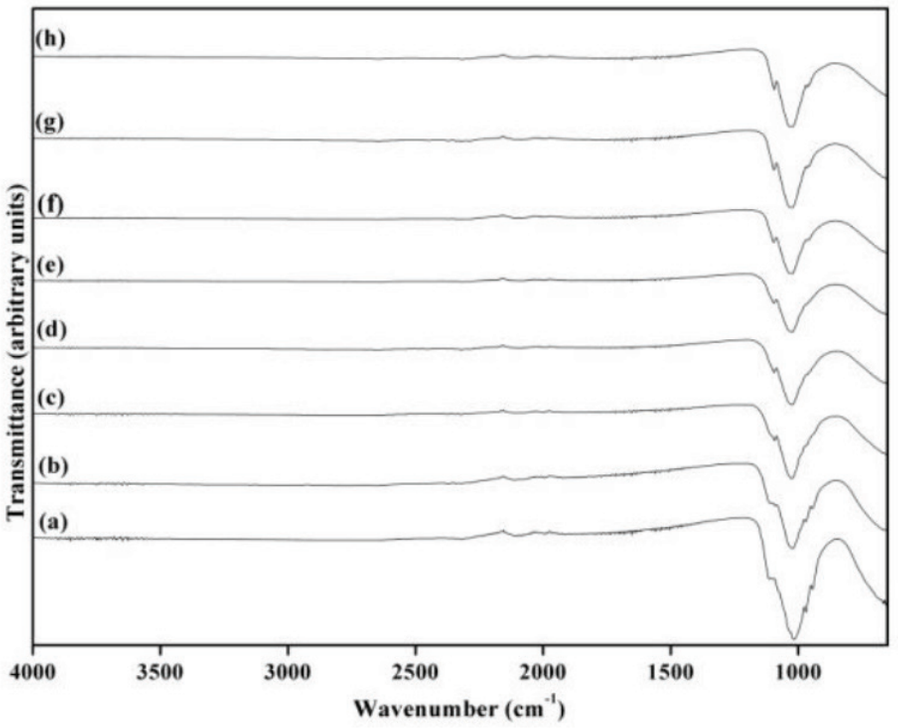

Figure 18. Infrared spectra of the TCP-40 wt% TiO_2 composites sintered at 1200°C for 1 h without and with different percentages of MgF_2: (a) 0 wt%, (b) 1 wt%, (c) 2.5 wt%, (d) 4 wt%, (e) 4.5 wt%, (f) 5 wt%, (g) 7.5 wt% and (h) 10 wt%.

http://dx.doi.org/10.5772/intechopen.68501

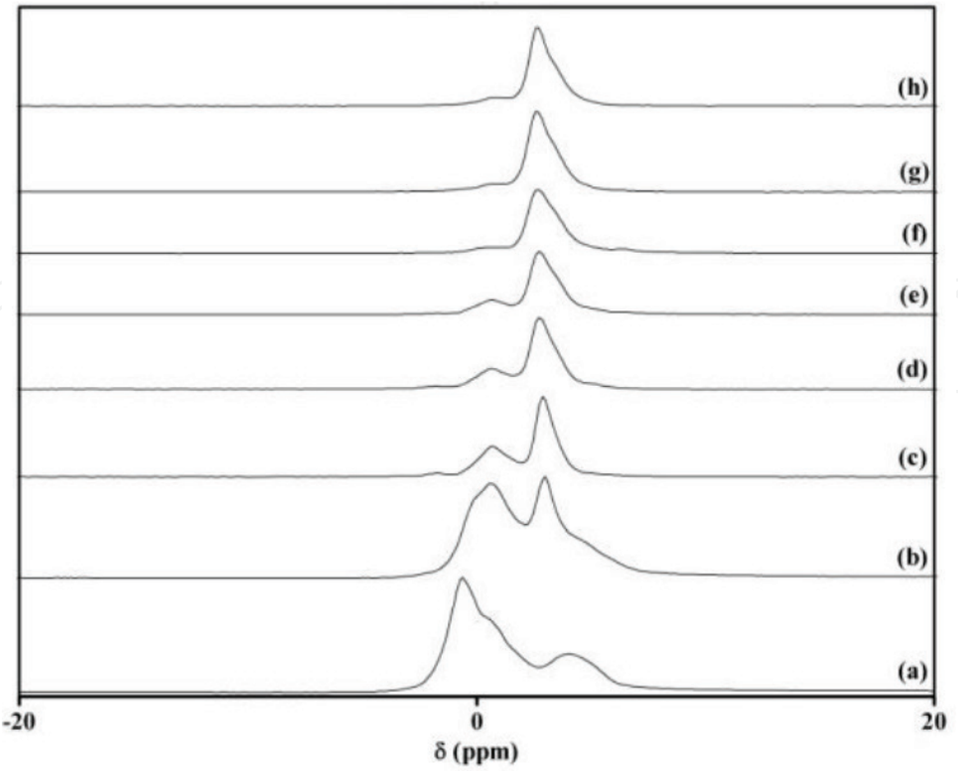

Figure 19. ^{31}P MAS-NMR spectra of the TCP-40 wt% TiO_2 composites sintered at 1200°C for 1 h without and with different percentages of MgF_2: (a) 0 wt%, (b) 1 wt%, (c) 2.5 wt%, (d) 4 wt%, (e) 4.5 wt%, (f) 5 wt%, (g) 7.5 wt% and (h) 10 wt%.

without and with different percentages of MgF_2 (2.5, 4, 7.5 and 10 wt%). The micrograph of the TCP-40 wt% TiO_2 composites sintered without MgF_2 depicts the coalescence of the grains of the TCP and the titania (**Figure 20a**). The microstructure of the TCP-40 wt% TiO_2 composites shows a liquid phase, a continuous phase relative to the β-TCP phases and a small-sized grain relative to the titania (**Figure 20a**). The morphology of the TCP=40 wt% TiO_2 composites sintered with 2.5 wt% MgF_2 was completely transformed (**Figure 20b**). This fact is explained by the intergranular porosity presence beside the grain growth and the formation of a new lamella form (**Figure 20b**). At higher amount of MgF_2 (4 wt%), this new phase still presented in the microstructure (**Figure 20c–d**). An important densification (94%) was registered after the addition of 4 wt% MgF_2 to the TCP-40 wt% TiO_2 composites (**Figure 20c–d**). This result can be explicated by the reduction in the porosity. Moreover, the microstructure of the TCP-38 wt% TiO_2-4 wt% MgF_2 composites shows continuous phases with dense contacts between the grains of the samples (**Figure 20c–d**). Both the addition of 7.5 and 10 wt% of MgF_2 led to the disappearance of the lamella form and the properties of the samples were hindered by the formation in the bubbles form and the grain growth in the microstructure (**Figure 20e–h**). Thus, the microstructure of the TCP-36.25 wt% TiO_2-7.5 wt% MgF_2 composites sintered at 1200°C presents the bubbles form (**Figure 20e–f**). Moreover, the micrographs of the TCP-35 wt% TiO_2-10 wt% MgF_2 depict the grains in hexagonal form formation beside the bubbles form (**Figure 20g–h**).

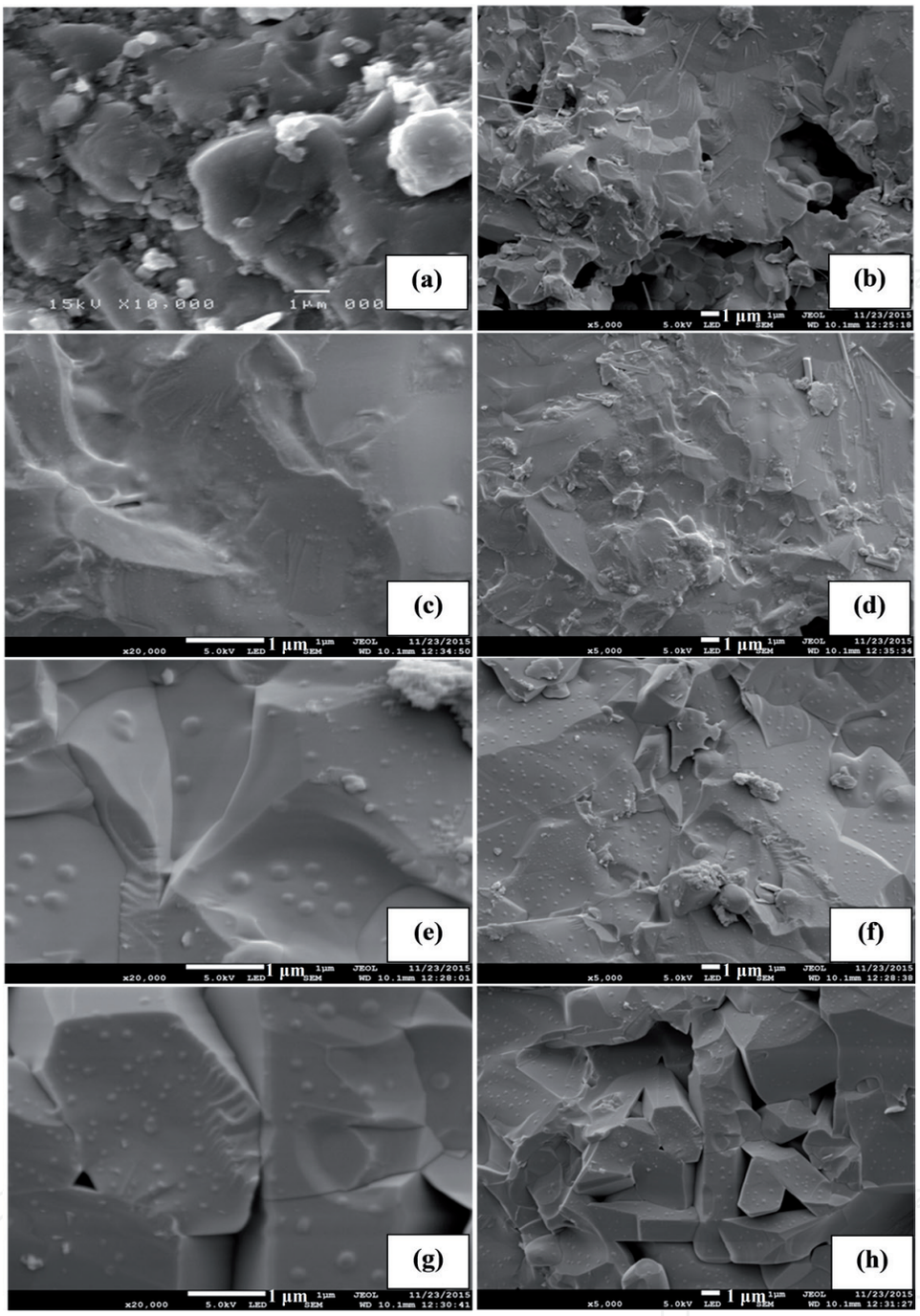

Figure 20. SEM micrographs of the TCP-40 wt% TiO_2 composites sintered at 1200°C for 1 h without and with different percentages of MgF_2: (a) 0 wt% (×10,000), (b) 2.5 wt% (×5000), (c) 4 wt% (×20,000), (d) 4 wt% (×5000), (e) 7.5 wt% (×20,000), (f) 7.5 wt% (×5000), (g) 10 wt% (×20,000) and (h) 10 wt% (×5000).

4. Discussion

In the light of its astonishing properties in terms of biocompatibility, in vivo bioactivity, osteoconductivity and bio-resorbability, tricalcium phosphate has been emerged as one of the most imperative biomaterials [6, 58, 59]. Many authors reported rather fast degradation

of the TCP while some researchers observed a minimal or very slow resorption [6, 59, 60]. Consequently, the addition of the inert oxide can enhance the mechanical performances of the TCP in order to combine the high mechanical and tricological properties of titania with the resorbability of TCP. The study of the tricalcium phosphate/titania system interested on improving the densification and the mechanical properties of the TCP by the addition of different amount of TiO_2. The properties of the TCP-TiO_2 composites were increased in accordance with the amount of titania and the sintered temperature. Thus, the optimum values of these composites were acquired after the sintering at 1200°C with 40 wt% of titania. The objective of this study aimed to ameliorate the performances of these composites by the addition of a reinforcement agent like magnesium fluoride (MgF_2). Recently, magnesium, as a dopant in both apatite and β-TCP structures, has been the subject of specific interest due to its important role in biological processes after implantation [61, 62]. Magnesium plays an essential role in the formation of dental caries and bone deposition. Magnesium ions promote bone mineralization and control the growth of the calcium phosphate crystals under in vivo conditions [62, 63]. Magnesium indirectly influences bone resorption and directly stimulates osteoblast proliferation with an effect comparable to that of insulin (a known growth factor for osteoblast) [62–64]. Thus, magnesium containing calcium phosphates is more appropriate for biomaterials and their applications [62]. Magnesium ions play important roles in the formation and transformation of biologically related calcium phosphates [65, 66]. MgF_2 ion is known as the most promising dental caries-promoting element due to a high initial calcification process in the bone formation [37, 38]. Also, fluoride is known to be important in suppressing dental caries [33, 34]. It stimulates the proliferation and the differentiation of bone cells [35]. The fluorine ion (F^-) has been investigated as an essential element for bone and dental formation in the human body [35, 36]. The effect of adding different percentages of MgF_2 on the mechanical properties of the TCP-40 wt% TiO_2 composites sintered at 1200°C for different lengths of the sintering time was investigated. The mechanical performances were studied by Vickers indentation, Brazilian test and ultrasound techniques to determine Vickers hardness (H), the mechanical strength (σ_r) and the elastic moduli (E and G), respectively. The mechanical properties of the TCP-40 wt% TiO_2 composites increase as in terms of the amounts of MgF_2. The optimum values (ρ = 94%, σ_r = 27 MPa, E = 51 GPa, G = 20 GPa and H = 360 Hv) of the TCP-40 wt% TiO_2 composites are attained after the sintering process at 1200°C for 1 h with the addition of 4 wt% MgF_2. These values are relatively similar to those of the bone tissues and precisely the enamel [6, 8, 67–70]. Thus, the enamel is mainly made of the mineral in the calcium phosphate [69, 71]. It is the hardest tissue in the human body because it contains almost no water [69]. For this reason, it is good to get a similar behavior as enamel. In fact, Chun et al. studied the mechanical properties of both enamel and dentin [69].

Therefore, if we compare the value of the strain and stress, enamel tend to fractures earlier than dentin, so it is more brittle than dentine. Nevertheless, if we compare from Vickers hardness value, the enamel is harder than dentine. In fact, dentin was characterized by a higher force resistance while enamel was characterized by a higher wear resistance [69]. The comparison between the previous work derived from the TCP-40 wt% TiO_2 composites and the present work, with adding MgF_2 (the TCP-38 wt% TiO_2-4 wt% MgF_2 composites) leads to the same conclusion described between enamel and dentin. However, as far as hardness is considered, the TCP-38 wt% TiO_2-4 wt% MgF_2 composites are considered harder than the TCP-40 wt%

TiO_2 composites. Such similarity between the present work and the enamel behaviors allows us to study the performances of the TCP-38 wt% TiO_2-4 wt% MgF_2 composites in biomedical applications and specifically as enamel.

The densification discrepancy of the samples prepared by a mixture of the TCP-40 wt% TiO_2 composites with adding 4 wt% MgF_2 (ϱ = 94%) and without MgF_2 (ϱ = 89%) may be due to different phenomena. Thus, the formation of the new compounds and the liquid phase gives rise to the performances of the composites. In general, the very important conditions for the densification by liquid phase sintering are the low viscosity of liquid for fast diffusion of solid through liquid and the solubility of solid to liquid [72] which is responsible for the significant improvement of these properties. Furthermore, several studies have shown the formation of the liquid phase during the sintering process of the tricalcium phosphate/titania system [12, 22]. Thus, Caroff et al. proved that a binary eutectic between the tricalcium phosphate and the titania is relative to this liquid phase [22]. So, in this study, there are two rate-controlling processes in the liquid phase sintering: the dissolution-precipitation phenomena which are dominant sintering mechanism in enhancing the densification by smoothing the contact interface and dissolution of the finer particles and the grain rearrangement occurs due to capillary force between particles. These results are confirmed by literature [72]. So, liquid phase sintering helps to fill the pore in the microstructure of the TCP-TiO_2-MgF_2 composites.

Several examples of the mechanical properties of the bone tissues are shown in **Table 4**. The optimum value of Vickers hardness of the TCP-40 wt% TiO_2 composites was obtained after the addition of 4 wt% MgF_2 (H = 360 Hv). If we compare this result with that of the TCP-40 wt% TiO_2 composites without adding the magnesium fluoride, we notice an increase from 270 to 360 Hv. So, adding 4 wt% MgF_2 enhances Vickers hardness of the TCP-40 wt% TiO_2 composites about 90 Hv. This value (H = 360 Hv) is so close to the value of the enamel (340–370 Hv) (**Table 4**).

Materials	H[a] (Hv)	E[b] (GPa)	G[c] (GPa)	References
Dentin	40–75	18	–	[6, 8, 69]
Enamel	340–370	50–82	–	[8, 69, 70]
Thigh bone	–	20	–	[6, 67, 68]
Cortical bone	–	7–25	–	[6, 67, 68]
β-TCP-40 wt% TiO_2 composites	270	33.1	15.7	Present work
β-TCP-38 wt% TiO_2-4 wt% MgF_2 composites	360	51	20	Present work

[a]Vickers hardness.

[b]Young's modulus.

[c]Shear modulus.

Table 4. Literature examples of the mechanical properties of the bone tissues.

The values of the elastic modulus (E and G) of the TCP-38 wt% TiO_2-4 wt% MgF_2 composites are close to those of the enamel (**Table 4**). In fact, the optimum values of the Shear modulus (G) and Young's modulus (E) of the composites reached 20 and 51 GPa, respectively. If we compare those values with the elastic modulus of the TCP-40 wt% TiO_2 composites sintered without MgF_2, we notice that the elastic corresponding modulus (E and G) of the composites sintered with 4 wt% MgF_2 increase generally about 18 GPa for Young's modulus and 4.3 GPa for the Shear modulus.

The evolution of the mechanical properties (E, G, H and σ_r) of the TCP-38 wt% TiO_2-4 wt% MgF_2 composites with different length of the sintering time is not improved. Thus, the optimum values of the mechanical properties (E = 51 GPa, G = 20 GPa, H = 360 Hv and σ_r = 27 MPa) are obtained after the sintering process for 1 h. In fact, for longer sintering dwell time, these properties are hindered. Indeed, we can retain that the performances (σ_r and H) of the TCP-38 wt% TiO_2-4 wt% MgF_2 composites sintered for 300 min or the TCP-35 wt% TiO_2-10 wt% MgF_2 composites sintered for 60 min are improved which is probably due to the formation of the FAp with more quantities in the TCP-TiO_2-MgF_2 composites. Consequently, the MgF_2 added to the TCP-TiO_2 composites structure enhances their performances with 4 wt%MgF_2.

The diffractograms of the TCP-40 wt% TiO_2 composites sintered at 1200°C with different percentages of MgF_2 indicate that the majority of peaks are relative to the rutile phase of titania (**Figure 17**). The spectrum of the TCP-40 wt% TiO_2 composites sintered without MgF_2 proves the presence of traces of $CaTiO_3$ and α-TCP besides the rutile phase and the β-TCP. The XRD spectra of the TCP-TiO_2-MgF_2 composites depicts the formation of both fluorapatite ($Ca_5(PO_4)_3F$) and $Mg_2(PO_4)F$ which is in agreement with the ^{31}P MAS-NMR analysis. Thus, the $Mg_2(PO_4)F$ was obtained only for 2.5, 4 and 4.5 wt% of MgF_2 and disappears for higher amounts of MgF_2 (**Figure 17**).This disappearance is attributed to the incorporation of this phase ($Mg_2(PO_4)F$) into the calcium phosphate structure by a solid state reaction through the compounds. The interaction between TCP and MgF_2 promotes the formation of the $Mg_2(PO_4)F$ and the fluorapatite ($Ca_5(PO_4)_3F$) according to the following reaction (Eq. (7)):

$$2Ca_3(PO_4)_{2(s)} + 2MgF_{2(s)} + TiO_{2(s)} + H_2O \leftrightarrow Ca_5(PO_4)_3F_{(s)} + CaTiO_{3(s)} + Mg_2(PO_4)F_{(s)} + 2HF_{(g)} \quad (7)$$

Several previous analyses (XRD and MAS-NMR) confirm the presence of these compounds [$Mg_2(PO_4)F$ and $Ca_5(PO_4)_3F$].

SEM analyses prove that excellent performances are attained with the TCP-38 wt% TiO_2-4 wt% MgF_2 composites sintered at 1200°C for 1 h. In fact, the continuous phases formed and the new compounds accompanied with the liquid phase appearance improved the performances of the TCP-38 wt% TiO_2-4 wt% MgF_2 composites. These results confirm those obtained with the XRD analysis. Thus, the new lamella form detected in the microstructure of the TCP-38 wt% TiO_2-4 wt% MgF_2 composites is probably accorded to the $Mg_2(PO_4)F$ derived from the solid reaction between MgF2 and TCP according to the previous reaction (Eq. (7)). Above 4 wt% MgF_2, the mechanical properties of the TCP-TiO_2-MgF_2 composites were hindered by the grain growth presence and the bubbles form in the microstructure of composites. Those

bubbles resulted from the HF gas evaporation according to the reaction (Eq. (7)). The micrograph of the TCP-35 wt% TiO_2-10 wt% MgF_2 composites indicates the hexagonal grain forms relative to the FAp formation. This phenomenon was accelerated by the dissolution-precipitation phenomena in the liquid phase. Therefore, the liquid phase sintering is used for homogenization and consolidation which presents the advantages of this production method. Thus, the densification of those composites resulted from three processes: the dissolution-precipitation, the rearrangement and the coalescence. This fact is previously confirmed by literature [72–74]. Generally, the microstructure of sintered body by liquid phase sintering mode includes secondary phase, which influences the mechanical, chemical and thermal properties.

5. Conclusion

The effect of the MgF_2 addition on the performances of the TCP-40 wt% TiO_2 composites was studied during the sintering process at 1200°C for different length of the sintering time. The addition of 4 wt% MgF_2 to the TCP-40 wt% TiO_2 composites led to a maximum of both the densification and the mechanical properties after the sintering process at 1200°C for 1 h. A notable amelioration in the elastic modulus and Vickers hardness of the TCP-40 wt% TiO_2 composites was attained with 4 wt% MgF_2 (E = 51 GPa, G = 20 GPa and H = 360 Hv). The enhancement of the composites properties resulted from the formation of new compounds and the liquid phase which permits to fill the pores in the microstructure. Thus, the microstructure indicates the presence of new lamella form relative to the $Mg_2(PO_4)F$ and the hexagonal grains relative to FAp. Above 4 wt% MgF_2, the properties of the composites are hindered by the grain growth formation and the presence of the bubbles form as a result of the dissolution-precipitation phenomena.

Author details

Ibticem Ayadi and Foued Ben Ayed*

*Address all correspondence to: benayedfoued@yahoo.fr

Laboratory of Industrial Chemistry, National Engineering School, Sfax University, Sfax, Tunisia

References

[1] Ben Ayed F, Chaari K, Bouaziz J, Bouzouita K. Frittage du phosphate tricalcique. Comptes Rendus Physique. 2006;**7**:825. DOI: 10.1016/j.crhy.2006.07.012

[2] Ben Ayed F. Elaboration and characterization of calcium phosphate biomaterial for biomedical application. Rosario Pignatello, editor. In: Handbook of Biomaterials—Physics and Chemistry: In Tech; 2011. pp. 357-374. DOI: 10.5772/23136

[3] Bouslama N, Ben Ayed F, Bouaziz J. Sintering and mechanical properties of tricalcium phosphate-fluorapatite composite. Ceramics International. 2009;**35**:1909-1917. DOI: 10.1016/j.ceramint.2008.10.030

[4] Bouslama N, Chevalier Y, Bouaziz J, Ben Ayed F. Influence of the sintering temperature on Young's modulus and the Shear modulus of tricalcium phosphate-fluorapatite composites evaluated by ultrasound techniques. Materials Chemistry and Physics. 2013;**141**:289-297. DOI: http://dx.doi.org/10.1016/j.matchemphys.2013.05.013

[5] Destainville A, Champion E, Bernache-Assolant D. Synthesis, characterization and thermal behavior of apatitic tricalcium phosphate. Materials Chemistry and Physics. 2003;**80**(1):269-277. DOI: 10.1016/S0254-0584(02)00466-2

[6] Elliott JC. Handbook of Structure and Chemistry of the Apatite and Other Calcium Orthophosphates. Vol. 18. Elsevier Science: BV; 1994. 404 p. ISBN: 9781483290317

[7] Gaasbeek RD, Toonen HG, Van Heerwaarden RJ, Buma P. Mechanism of bone incorporation of β-TCP bone substitute in open wedge tibial osteotomy in patients. Biomaterials. 2005;**26**:6713-6719. DOI: http://dx.doi.org/10.1016/j.biomaterials.2005.04.056

[8] Hench LL. Handbook of an Introduction to Bioceramics, Chapter 37: Characterization of Bioceramics. Hench LL and Wilson J, editors, World Scientific Publishing Co Pte Ltd; Singapore, 1993. pp. 521-540. ISBN: 9789814504164

[9] Hench LL. Bioceramics. Journal of the American Ceramic Society. 1998;**7**:1705-1728. DOI: 10.1111/j.1151-2916.1998.tb02540.x

[10] Jensen SS, Broggini N, Hjorting-Hansen E, Schenk R, Buser D. Bone healing and graft resorption of autograft, anorganic bovine bone and beta-tricalcium phosphate, a histologic and histomorphometric study in the mandibles of minipigs. Clinical Oral Implants Research. 2006;**17**:237-243

[11] Sakka S, Bouaziz J, Ben Ayed F. Mechanical properties of biomaterials based on calcium phosphates and bioinert oxides for applications in biomedicine. Rosario Pignatello, editor. Handbook of Advances in Biomaterials Science and Biomedical Applications. InTech; 2013. pp. 23-50. DOI: 10.5772/53088

[12] Sakka S, Bouaziz J, Ben Ayed F. Sintering and mechanical properties of the alumina-tricalcium phosphate-titania composites. Materials Science and Engineering C. 2014;**40**:92-101. DOI: 10.1016/j.msec.2014.03.036

[13] Sallemi I, Bouaziz J, Ben Ayed F. The effect of adding magnesium oxide on the mechanical properties of the tricalcium phosphate-zirconia composites. Materials Chemistry and Physics. 2015;**151**:50-59. http://dx.doi.org/10.1016/j.matchemphys.2014.11.027 DOI:10.1016/j.matchemphys.2014.11.027#doilink

[14] Sallemi I, Bouaziz J, Ben Ayed F. Elaboration and characterization of bioceramic based on tricalcium phosphate and zirconia. International Journal of Current Engineering and Technology. 2013;**28**:1691-1700. ISSN 2277-4106

[15] Runyan JL, Bennison SJ. Fabrication of flaw-tolerant aluminium titanate-reinforced alumina. Journal of the European Ceramic Society. 1991;**7**:93-99. DOI: 10.1016/0955-2219(91)90006-L DOI:10.1016/0955-2219(91)90006-L#_blank#Persistent link using digital object identifier

[16] Jung S, Kim JH. Sintering characteristics of TiO_2 nanoparticles by microwave processing. Korean Journal of Chemical Engineering. 2010;**27**:645-650. DOI: 10.1007/s11814-010-0057-2

[17] Kaneko H, Uchida M, Kokubo T, Nakamura T. Process of apatite formation induced by anatase on titanium metal in simulated body fluid. In: Brown S, Clarke IC, Williams P, editors. Handbook of Bioceramics 14. Trans Tech Publications Key Engineering Materials; Switzerland, 2002. pp. 649-652. ISBN: 9780878498895

[18] Li D, Chen S, Jing Y, Shao W, Zhang Y, Luan W. The Master sintering curve for pressureless sintering of TiO_2. Science of Sintering. 2007;**39**:103-110. DOI: 10.2298/SOS0702103L

[19] Mazaheri M, Zahedi AM, Haghighatzadeh M, Sadrnezhaad SK. Sintering of titania nanoceramic: densification and grain growth. Ceramics International. 2009;**35**:685-691. DOI: http://dx.doi.org/10.1016/j.ceramint.2008.02.005 DOI:10.1016/j.ceramint. 2008.02.005#doilink

[20] Shin CK, Paek YK. Effect of CuO on the sintering behavior and dielectric characteristics of titanium dioxide. International Journal of Applied Ceramic Technology. 2006;**3**:463-469. DOI: 10.1111/j.1744-7402.2006.02106.x

[21] Ning CQ, Zhou Y. In vitro bioactivity of a biocomposite fabricated from HA and Ti powders by powder metallurgy method. Biomaterials. 2002;**23**:2909-2915. DOI: http://dx.doi.org/10.1016/S0142-9612(01)00419-7 DOI:10.1016/S0142-9612(01)00419-7#doilink

[22] Caroff F, Oh KS, Famery R, Boch P. Sintering of TCP-TiO_2 biocomposites: Influence of secondary phases. Biomaterials. 1998;**19**:1451-1454. DOI: 10.1016/S0142-9612(98)00057-X DOI:10.1016/S0142-9612(98)00057-X#_blank#Persistent link using digital object identifier

[23] Lee JK, Seo DS, Jung HC. Densification and sintering of tricalcium phosphate/titania composite by hot pressing. In: Handbook of the Science of Engineering Ceramics III. T. Ohji, T. Sekino and K. Niihara, editors. Trans Tech Publications Key Engineering Materials; Switzerland, 2006. pp. 101-104. DOI: 10.4028/ www.scientific.net/KEM.317-318.101

[24] Sprio S, Guicciardi S, Dapporto M, Melandri C, Tampieri A. Synthesis and mechanical behavior of β-tricalcium phosphate/titania composites addressed to regeneration of long bone segments. Journal of Mechanical Behavior of Biomedical Materials. 2013;**17**:1-10. DOI: http://dx.doi.org/10.1016/j.jmbbm.2012.07.013 DOI:10.1016/j.jmbbm.2012.07.013#doilink

[25] Manujubala I, Sampath Kumar TS. Preparation of biphasic calcium phosphate doped with magnesium fluoride for osteoporotic applications. Journal of Materials Science Letters. 2001;**20**:1225-1227. DOI: 10.1023/A:1010926923815

[26] Haines J, Leger JM, Gorelli F, Klug DD, Tse JS, Li ZQ. X-ray diffraction and theoretical studies of the high-pressure structures and phase transitions in magnesium fluoride. Physical Review B. 2001;**64**:134110-134131. DOI: https://doi.org/10.1103/PhysRevB.64.134110

[27] Kanchana V, Vaitheeswaran G, Rajagopalan M. High pressure structural phase transitions in magnesium fluoride studied by electronic structure calculations. Journal of Alloys and Compounds. 2003;**352**:60-65. DOI: http://dx.doi.org/10.1016/S0925-8388(02)01158-1 DOI:10.1016/S0925-8388(02)01158-1#doilink

[28] Kusaba K, Kikegawa T. Stable phase with the α-PbO_2 type structure in MgF_2 under high pressure and high temperature. Solid State Communications. 2008;**148**:440-443. DOI: 20081218287

[29] Sun XW, Song T, Liu ZJ, Zhang CR, Tian JH, Guo P. High-pressure and high-temperature bulk modulus of cubic fluorite-type MgF_2 from quasi-harmonic Debye model. Solid State Communications. 2011;**151**:1507-1510. DOI: http://dx.doi.org/10.1016/j.ssc.2011.07.040 DOI:10.1016/j.ssc.2011.07.040#doilink

[30] Babu KR, Lingam CB, Auluck S, Tewari SP, Vaitheeswaran G. Structural, thermodynamic and optical properties of MgF2 studied from first-principles theory. Journal of Solid State Chemistry. 2011;**184**:343-350. DOI: http://dx.doi.org/10.1016/j.jssc.2010.11.025 DOI:10.1016/j.jssc.2010.11.025#doilink

[31] Ozturk H, Kurkcu C, Kurkcu C. High-pressure structural phase transitions and intermediate phases of magnesium fluoride. Journal of Alloys and Compounds. 2014;**597**: 155-160. DOI: http://dx.doi.org/10.1016/j.jallcom.2014.01.221 DOI:10.1016/j.jallcom.2014.01.221#doilink

[32] Ozturk H, Kurkcu C, Kurkcu C. Structural phase transformations and new intermediate phases of MgF_2 under high-pressures applied via conjugate-gradient method. Journal of Alloys and Compounds. 2014;**609**:185-191. DOI: http://dx.doi.org/10.1016/j.jallcom.2014.04.152 DOI:10.1016/j.jallcom.2014.04.152#doilink

[33] Nakade O, Koyama H, Arai J, Ariji H, Takad J, Kaku T. Stimulation by low concentrations of fluoride of the proliferation and alkaline phosphatase activity of human dental pulp cells in vitro. Archives of Oral Biology. 1999;**44**:89-92. DOI: 10.1016/S0003-9969(98) 00099-5

[34] Evis Z, Pinar Sun Z. Structural and mechanical investigations of magnesium and fluoride doped nanosize calcium phosphates. Journal of Ceramic Processing Research. 2010;**11**(6):701-715

[35] Farley JR, Wergedal JE, Baylink DJ. Fluoride directly stimulates proliferation and alkaline phosphatase activity of bone-forming cells. Science. 1983;**222**(4621):330-332. DOI: PMID:6623079

[36] Fathi MH, Zahrani EM. The effect of rotation speed and time of milling on synthesis and properties of fluoridated hydroxyapatite biomaterial. Iranian Journal of Pharmaceutical Science. 2008;**4**(3):201-208. ISSN: 1735-2444

[37] Kim SH, Lee HC, Bang HG, Park SY. Effect of MgF_2 additive on the mechanical properties in Hydroxyapatite/Zirconia composites. In: Handbook of Eco-Materials Processing & Design VII. Hyung Sun Kim, Yu Bao Li and Soo Wohn Lee, editors. Trans Tech Publications Materials Science Forum; Switzerland, 2006. pp. 478-481. DOI: 10.4028/www.scientific.net/MSF.510-511.478

[38] Gu XN, Zheng YF. A review on magnesium alloys as biodegradable materials. Frontiers of Materials Science in China. 2010;**4**(2):111-115. DOI: 10.1007/s11706-010-0024-1

[39] Xue W, Dahlquist K, Banerjee A, Bandyopadhya A, Bose S. Synthesis and characterization of tricalcium phosphate with Zn and Mg based dopants. Journal of Materials Science: Materials in Medicine. 2008;**19**:2669-2677. DOI: 10.1007/s10856-008-3395-4

[40] Chang CS, Hon MH. Texture effect of hot-pressed magnesium fluoride on optical transmittance. Materials Chemistry and Physics. 2003;**81**(1):27-32. DOI: http://dx.doi.org/10.1016/S0254-0584(02)00460-1

[41] Nofar M, Madaah Hosseini HR, Shivaee HA. The dependency of optical properties on density for hot pressed MgF_2. Infrared Physics and Technology. 2008;**51**:546-549. DOI: http://dx.doi.org/10.1016/j.infrared.2008.06.002 DOI:10.1016/j.infrared.2008.06.002#doilink

[42] Evis Z, Usta M, Kutbay I. Improvement in sinterability and phase stability of hydroxyapatite and partially stabilized zirconia composites. Journal of the European Ceramic Society. 2009;**29**:621-628. DOI: http://dx.doi.org/10.1016/j.jeurceramsoc.2008.07.020 DOI: 10.1016/j.jeurceramsoc.2008.07.020#doilink

[43] Pardun K, Treccani L, Volkmann E, Streckbein P, Heiss C, Gerlach JW, Maendl S, Rezwan K. Magnesium containing mixed coatings on zirconia for dental implants: Mechanical characterization and in vitro behavior. Journal of Biomaterials Applications. 2015;**30**(1):104-118. DOI: 10.1177/0885328215572428

[44] Chen X, Chen X, Brauer DS, Wilson RM, Hill RG, Karpukhina N. Novel alkali free bioactive fluorapatite glass ceramics. Journal of Non-Crystalline Solids. 2014;**402**:172-177. DOI: 10.1016/j.jnoncrysol.2014.05.025

[45] Kanazawa T, Umegaki T, Yamashita K, Monma H, Hiramatsu T. Effects of additives on sintering and some properties of calcium phosphates with various Ca/P Ratios. Journal of Materials Science. 1991;**26**:417-422. DOI: 10.1007/BF00576536

[46] Hench LL. Bioceramics: From concept to clinic. Journal of the American Ceramic Society. 1991;**74**:1487-1510. DOI: 10.1111/j.1151-2916.1991.tb07132.x

[47] Azami M, Jalilifiroozinezhad S, Mozafari M, Rabiee M. Synthesis and solubility of calcium fluoride/hydroxy-fluorapatite nanocrystals for dental applications. Ceramics International. 2011;**37**:2007-2014. DOI: http://dx.doi.org/10.1016/j.ceramint.2011.02.025 DOI:10.1016/j.ceramint.2011.02.025#doilink

[48] Carsten J, Marco B. ^{19}F NMR spectroscopy of glass ceramics containing fluorapatites. Biomaterials.1996;**17**(21):2065-2069. PMID: 8902239

[49] Sakka S, Ben Ayed F, Bouaziz J. Mechanical properties of tricalcium phosphate alumina composites. Cheikhrouhou A, editor. In: Proceedings of the IOP Conference Series on Materials Science and Engineering. Mahdia Tunisia, 2012;**28**:012028. DOI:10.1088/1757-899X/28/1/012028

[50] Brunauer S, Emmet PH, Teller J. Adsorption of gases in multimolecular layers. Journal of the American Chemical Society. 1938;**60**:310-319. DOI: 10.1021/ja01269a023

[51] Bernache-Assollant D. Handbook of Chimie-physique du Frittage Forceram Formation Céramique. 1st ed. Lavoisier: Hermès Science Publications; 1993. 345 p. ISBN: 9782866013431

[52] ASTM C496. Standard test method for splitting tensile strength of cylindrical concrete specimens. In: Annual Book of ASTM Standards. Philadelphia: ASTM; 1984. p. 336. DOI: 10.1520/C0496_C0496M-11

[53] ISRM. Suggested methods for determining tensile strength of rock materials. International Journal of Rock Mechanics and Mining Sciences and Geomechanics Abstracts. 1978;**15**:99-103. DOI: 10.1016/0148-9062(78)91677-7 DOI:10.1016/0148-9062(78)91677-7#_blank#Persistent link using digital object identifier

[54] ASTM C1327-96. Standard test method for Vickers indentation hardness of advanced ceramics. In: Annual Book of ASTM Standards. West Conshohocken, United States, 2003

[55] Chevalier Y. Essais dynamiques sur composites—caractérisation aux hautes fréquences. Techniques de l'Ingénieur. 2003. pp. 1-19. REF:AM5401 V1

[56] Bouslama N, Ben Ayed F, Bouaziz J. Effect of fluorapatite additive on densification and mechanical properties of tricalcium phosphate. Journal of the Mechanical Behavior of Biomedical Materials. 2010;**3**:2-13. DOI: http://dx.doi.org/10.1016/j.jmbbm.2009.01.007 DOI: 10.1016/j.jmbbm.2009.01.007#doilink

[57] Gouma PI, Mills MJ. Anatase to rutile transformation in titania powders. Journal of the American Ceramic Society. 2001;**84**:619-622. DOI: 10.1111/j.1151-2916.2001.tb00709.x

[58] Vallet-Regi M, Gonzalez-Calbet JM. Calcium phosphates as substitution of bone tissues. Progress in Solid State Chemistry. 2004;**32**:1-31. DOI: http://dx.doi.org/10.1016/j.progsolidstchem.2004.07.001 DOI: 10.1016/j.progsolidstchem.2004.07.001#doilink

[59] Williams D. An introduction to medical and dental materials. In: Williams D, editor. Concise Encyclopedia of Medical and Dental Materials. Pergamon Press and the MIT Press. Pergamon, 1990. pp. xvii-xx

[60] LeGeros RZ, LeGeros JP, Daculsi G, Kijkowaka R. Calcium phosphate biomaterials: Preparation, properties, and biodegradation. In: Wise DL, Trantolo DJ, Altobelli DE, et al., editors. Encyclopedic Handbook of Biomaterials and Bioengineering, Part A: Materials. New York: Marcel Dekker; 1995. pp. 1429-1463

[61] Kannan S, Neunhoeffer FG, Neubauer J, Rebelo AHS, Valério P, Ferreira JMF. Rietveld structure and in vitro analysis on the influence of magnesium in biphasic hydroxyapatite and β-tricalcium phosphate mixtures. Journal of Biomedical Materials Research Part B: Applied Biomaterials. 2009;**90**(1):1552-4981. DOI: 10.1002/jbm.b.31299

[62] Gozalian A, Behnamghader A, Daliri M, Moshkforoush A. Synthesis and thermal behavior of Mg-doped calcium phosphate nanopowders via the sol gel method. Scientia Iranica Transactions F: Nanotechnology. 2011;**18**(6):1614-1622. DOI: 10.1016/j.scient.2011.11.014

[63] Serre CM, Papillard M, Chavassieux P, Voegel JC, Boivin G. Influence of magnesium substitution on a collagen-apatite biomaterial on the production of a calcifying matrix by human osteoblasts. Journal of Biomedical Materials Research. 1998;**42**:626-633. DOI: 10.1002/(SICI)1097-4636(19981215)42:4<626::AID-JBM20>3.0.CO;2-S

[64] Suchanek WL, Byrappa K, Shuk P, Riman RE, Janas VF, TenHuisen KS. Mechanochemical-hydrothermal synthesis of calcium phosphate powders with coupled magnesium and carbonate substitution. Journal of Solid State Chemistry. 2004;**177**:793-799. DOI: http://dx.doi.org/10.1016/j.jssc.2003.09.012 DOI:10.1016/j.jssc.2003.09.012#doilink

[65] LeGeros RZ. Calcium phosphates in oral biology and medicine. In: Myers HM, editor. Handbook of Monographs in Oral Sciences.1st ed. Basel: Karger; 1991. pp. 1-200. PMID: 1870604

[66] Otsuka M, Oshinbe A, LeGeros RZ, Tokudome Y, Ito A, Otsuka K, Higuchi WI. Efficacy of the injectable calcium phosphate ceramics suspensions containing magnesium, zinc and fluoride on the bone mineral deficiency in ovariectomized rats. Journal of Pharmaceutical Sciences. 2008;**97**(1):421-432. DOI: 10.1002/jps.21131

[67] Ravaglioli A, Krajewski A. Handbook of Bioceramics: Materials, Properties and Appli cations. London, England: Chapman & Hall; 1992. 422 p. DOI: 10.1007/97 8-94-011-2 336-5

[68] Shi D, editor. Handbook of Biomaterials and Tissue Engineering. 1st ed. New York: Springer-Verlag Berlin Heidelberg; 2004. 200 p. DOI: 10.1007/978-3-662-06104-6

[69] Chun KJ, Choi HH, Lee JY. Comparison of mechanical property and role between enamel and dentin in the human teeth. Journal of Dental Biomechanics. 2014;**5**:1-6. DOI: 10.1177/1758736014520809 DOI:10.1177%2F1758736014520809#pmc_ext

[70] Biswas N, Dey A, Kundu S, Chakraborty H, Mukhopadhyay AK. Mechanical properties of enamel nanocomposite. ISRN Biomaterials Hindawi. 2013;**2013**:1-15. DOI: http://dx.doi.org/10.5402/2013/253761

[71] Staines M, Robinson WH, Hood JAA. Spherical indentation of tooth enamel. Journal of Materials Science. 1981;**16**(9):2551-2556. DOI: 10.1007/BF01113595

[72] Hosokawa M, Nogi K, Naito M, Yokoyama T, editors. Handbook of Nanoparticle Technology. 1st ed. Linacre House, Amsterdam, The Netherlands: Elsevier BV; 2007. 644 p. ISBN: 9780080558028

[73] Ben Ayed F, Bouaziz J, Bouzouita K. Pressureless sintering of Fluorapatite under oxygen atmosphere. Journal of the European Ceramic Society. 2000;**20**(8):1069-1076. DOI: 10.1016/S0955-2219(99)00272-1

[74] Ben Ayed F, Bouaziz J, Bouzouita K. Calcination and sintering of fluorapatite under argon atmosphere. Journal of Alloys and Compounds. 2001;**322**(1-2):238-245. DOI: http://dx.doi.org/10.1016/S0925-8388(01)01200-2 DOI:10.1016/S0925-8388(01)01200-2#doilink